Insect Systematics and Diversity, (2020) 4(6): 1; 1–29
doi: 10.1093/isd/ixaa013
Research

Phylogenomic and Morphological Reevaluation of the Bee Tribes Biastini, Neolarrini, and Townsendiellini (Hymenoptera: Apidae) With Description of Three New Species of *Schwarzia*

Silas Bossert,[1,2,8] Robert S. Copeland,[2,3] Trevor J. L. Sless,[4] Michael G. Branstetter,[5] Jessica P. Gillung,[6] Seán G. Brady,[2] Bryan N. Danforth,[1] Jana Policarová,[7] and Jakub Straka[7]

[1]Department of Entomology, Cornell University, Comstock Hall, Ithaca, NY 14853, [2]Department of Entomology, National Museum of Natural History, Smithsonian Institution, Washington, DC 20560, [3]ICIPE, International Centre of Insect Physiology and Ecology, Nairobi 00100, Kenya, [4]Department of Ecology and Evolutionary Biology, Cornell University, Corson Hall, Ithaca, NY 14853, [5]USDA, Agricultural Research Service, Pollinating Insects Research Unit, Utah State University, Logan, UT 84322, [6]Department of Natural Resource Sciences, McGill University, Sainte-Anne-de-Bellevue, Canada, [7]Department of Zoology, Faculty of Science, Charles University, CZ-12844 Prague, Czech Republic, and [8]Corresponding author, e-mail: sb2346@cornell.edu

Subject Editor: Bonnie Blaimer

Received 23 April, 2020; Editorial decision 24 August, 2020

Abstract

Bees of the tribes Biastini, Neolarrini, and Townsendiellini are cleptoparasites in the subfamily Nomadinae (Hymenoptera, Apidae) and parasitize solitary bees. Understanding their phylogenetic relationships has proven difficult for many decades. Previous research yielded ambiguous results because of conflicting phylogenetic signals of larval and adult morphological characters. Molecular data settled some of this disparity but our knowledge remains fragmented due to limited taxon sampling and the discovery of a new lineage associated with Biastini: the enigmatic *Schwarzia* Eardley, 2009. *Schwarzia* has unusual morphological features and seems transitional between previously established taxa. This puts limits on our ability to diagnose the groups, understand their antiquity and biogeography, and study the evolution of host-choice. To address this, we integrate phylogenomics and morphology to establish a fossil-calibrated phylogeny for the tribes Biastini, Neolarrini, and Townsendiellini. We show that *Schwarzia* is indeed closely related to *Biastes* Panzer, 1806, but *Biastes* itself is paraphyletic in respect to *Neopasites* Ashmead, 1898, and even Biastini is paraphyletic due to *Townsendiella* Crawford, 1916, which is sister to *Rhopalolemma* Roig-Alsina, 1991. To ensure monophyly, we lower *Neopasites* to subgeneric rank within *Biastes* and resurrect *Melittoxena* Morawitz, 1873 as a third subgenus. We then assess the diagnosability of different tribal concepts and establish an expanded tribe Neolarrini that includes Biastini and Townsendiellini as new synonyms for Neolarrini. Neolarrini in this new, expanded sense likely originated in the Nearctic in the mid-Eocene and is, as far we know, composed exclusively of parasites of oligolectic hosts. Lastly, our continued efforts to find the rare *Schwarzia* in Eastern Africa led to the discovery of three new species, which are described herein.

Key words: ultraconserved element, cleptoparasitism, Eastern Africa, biogeography, host–parasite pattern

The small bee tribe Biastini, Linsley and Michener (1939), was established to include the two genera currently known as *Biastes* Panzer, 1806 and *Neopasites* Ashmead, 1898. They are in the subfamily Nomadinae (Apidae) and are, as far as we know, all cleptoparasites in nests of rophitine sweat bees (Halictidae, Rophitinae). As of now, we know of five described species of *Neopasites* from the Nearctic and five *Biastes* from the Palearctic (Ascher and Pickering 2020). They have intriguingly specific host-choices and all their known hosts are strict pollen specialists. Documented hosts comprise bees in the genera *Dufourea* Lepeletier, 1841, *Rophites* Spinola, 1808, or *Systropha* Illiger, 1806 (e.g., Michener 2007, Scheuchl and Willner 2016, Westrich 2018).

Biastes and *Neopasites* are morphologically very similar in their adult and larval morphology, but phylogenetic relationships to other tribes of Nomadinae have proved difficult to establish for a long time. A general problem lies in the seemingly decoupled phylogenetic signal of different life stages, as larval and adult morphological

Version of Record, first published online November 12, 2020 with fixed content and layout in compliance with Art. 8.1.3.2 ICZN.

characters consistently supported different topologies. Early and recent comparative study of larvae indicated a close relationship to the minute *Neolarra* Ashmead, 1890, the sole genus of Neolarrini Fox, 1894 (Rozen 1966, Rozen et al. 1978, Straka and Bogusch 2007). Cladistic analyses further showed morphological similarities of larvae to those of another monogeneric tribe, Townsendiellini Michener, 1944 (Rozen and McGinley 1991, Rozen 1996, Rozen et al. 1997). Studies using adult morphology, however, did not recover a particularly close relationship of either *Neolarra* or *Townsendiella* Crawford, 1916 to Biastini (Roig-Alsina 1991, Rozen 1996; but see Alexander 1990). Instead, Roig-Alsina (1991) discovered the rare previously undescribed genus *Rhopalolemma* Roig-Alsina, 1991 and assigned it to Biastini.

The advent of molecular sequence data settled some of this disparity. Multigene and total-evidence studies generated topologies similar to those obtained from larval characters, recovering a clade comprising Biastini and Townsendiellini as sister group to Neolarrini (Cardinal et al. 2010, Litman et al. 2013, Payne 2014, Policarová et al. 2019). However, our understanding of the phylogenetic relationships among these groups remains fragmented, as recent discoveries and restricted taxon sampling limit our ability to diagnose the groups, understand their antiquity and historical biogeography, and study the evolution of host-choice in a comparative framework. Specifically, three central problems persist. First, it is unclear if *Neopasites* and *Biastes* are monophyletic groups. They have been synonymized previously (Warncke 1982) and certain morphological features of the sting apparatus render *Biastes* paraphyletic with respect to *Neopasites* (Roig-Alsina 1991). Michener's (2007) classification recognizes the genera with the notion that they may be 'only subgenerically distinct' and a little-known work in Russian plausibly suggested to divide *Biastes* into subgenera and recognize the long synonymized name *Melittoxena* Morawitz, 1873 as a subgenus (Popov 1933). Currently available molecular phylogenies do not allow us to address these issues, as studies included only single representatives of each genus. Second, the phylogenetic position of *Rhopalolemma* is uncertain. There is support for inclusion in Biastini (Roig-Alsina 1991), but typical morphological features are missing and cladistic analyses of larval characters suggested a closer relationship to *Townsendiella* (Rozen et al. 1997). Molecular sequence data could clarify phylogenetic affinities but are not yet available for *Rhopalolemma*. Lastly, the recently discovered genus *Schwarzia* Eardley, 2009 not only challenges our concept of the tribe Biastini but implies a dramatically greater biogeographical distribution than previously thought (Eardley 2009). *Schwarzia* has enigmatic, highly derived morphological features, and lacks certain tribal characters of Biastini, yet it resembles the tribe more strongly than other groups (Eardley 2009, Bossert 2019). The presumably closely related *Neopasites* and *Biastes* are Holarctic, whereas *Schwarzia* is only known from a few sites in Eastern Africa, presenting a biogeographical puzzle that cannot be understood without robust molecular phylogenetic data.

In order to address these issues and gain a comprehensive understanding of the natural history of these bees, we integrate phylogenomic analyses with morphological study of larval and adult characters. We establish the first fossil-calibrated molecular phylogeny including all relevant groups, provide information on ancestral ranges, and discuss the presently known host-associations. Using our well-supported topology, we reevaluate existing taxonomic classifications and propose a rank-based taxonomy of readily diagnosable, monophyletic groups. Lastly, our continued efforts to find specimens of the rare *Schwarzia* in Eastern Africa led to the discovery of three new species which are described herein.

Materials and Methods

Taxon Sampling

For our molecular phylogenetic study, we developed a comprehensive sampling of all known groups of Biastini and lineages that were considered closely related by morphological or molecular data (Table 1). Specifically, we obtained specimens for both known species of *Schwarzia* and included the three species that are newly described herein. We included two species of the North American *Neopasites* and three representatives of *Biastes*, including species that were previously placed in *Biastes* s. str. and *Melittoxena* (Popov 1933, Proshchalykin and Lelej 2004). In order to provide a framework for evaluating the phylogeny of these lineages within Nomadinae, we included all nomadine samples from a recent phylogenomic study of Apidae (Bossert et al. 2019), and additionally sequenced representatives of the Nearctic *Townsendiella*, *Neolarra*, and *Oreopasites* Cockerell, 1906.

For morphological study, we examined the same set of specimens and additional representatives of the subgenera *Micropasites* Linsley, 1942 and *Phileremulus* Cockerell, 1895, and compared the assessed character states to a previously published matrix of morphological characters of Apidae (Policarová et al. 2019).

Molecular Methods and Bioinformatic Processing

As *Schwarzia* is generally very rare, DNA was extracted with minimally destructive methods. We generally soaked single whole specimens in Proteinase-K extraction buffer from DNeasy Blood and Tissue Kits (Qiagen Inc.) and incubated overnight at 56°C (~12 h). After incubation, whole specimens were washed in ethanol and mounted back on pins. For the single specimen of *S. lualenyiensis*, which represents the holotype for the new species, we carefully broke off a single hindleg and glued it back on to the specimen after incubation. We followed the extraction kit manufacturer's protocol but eluted the DNA from the spin column with 120 µl of purified H_2O. For a few samples, we followed a similar nondestructive procedure, but used a standard phenol–chloroform isolation method.

Genomic library preparation and UCE enrichment were performed in two laboratories with very similar but slightly different protocols (differences noted below). Following extraction, we assessed DNA fragmentation and concentration, and sheared fragments to a targeted size of 450–600 bp using a Q800R sonicator (Qsonica, LLC.). We used up to 100 ng of DNA per sample to prepare individual dual-indexed libraries with a KAPA HyperPrep kit (Roche Sequencing Systems, Inc.) and Illumina TruSeq-style adapters (Glenn et al. 2019). For enrichment, we either followed the pooled on-bead enrichment procedure outlined in Faircloth et al. (2015), including the modifications from Blaimer et al. (2016a,b; laboratory 1), or we followed Arbor Biosciences v4 protocol for day 1 and the protocol above for day 2 (laboratory 2). We performed all UCE enrichments using the expanded Hymenoptera UCE bait set ('principal hym-v2 bait as described in Branstetter et al. 2017; laboratory 1') or a bee-ant-specific version of the bait set (described in Grab et al. 2019; laboratory 2), both synthesized by Arbor BioSciences (formerly MYcroarray Inc.). Following post-enrichment amplifications, in one laboratory (laboratory 1), we measured DNA quantity with a Qubit fluorometer (model 3.0, Thermo Fisher Scientific, Inc.) and assessed fragment distribution with an Agilent 2200 TapeStation and D1000 HS screen tapes (Agilent Technologies, Inc.). Based on the results, we combined pools at equimolar concentrations and size selected for a range of 250–600 bp with a Blue Pippin device (Sage Science, Inc.). In the other laboratory (laboratory 2), we measured DNA quantity with Qubit, examined fragment distributions

Table 1. Taxon sampling

Species	Collection locality	Voucher deposition	No. of captured UCE loci	NCBI SRA ID
Neolarrini (focal group; generated with Hymenoptera bait set v2)				
Biastes (*Biastes*) *brevicornis* (Panzer, 1798) [2]	Hungary, Budaörs, 3km W Budapest	Coll. Straka, Charles Univ.	2,299	SRR11497539
Biastes (*Biastes*) *emarginatus* (Schenck, 1870) [2]	Czech Republic, Bohemia, Prague	Coll. Straka, Charles Univ.	2,344	SRR11497547
Biastes (*Melittoxena*) *truncatus* (Nylander, 1848) **comb. nov.** [2]	Czech Republic, Bohemia, Vraný nad Vltavou	Coll. Straka, Charles Univ.	2,342	SRR11497542
Biastes (*Neopasites*) *cressoni* (Crawford, 1916) **comb. nov.** [1]	Mexico, Sonora, Rancho Puerta Blanca	Coll. Minckley, Univ. Rochester	1,421	SRR11497541
Biastes (*Neopasites*) sp. aff. *cressoni* [2]	USA, AZ, Cochise Co., 11.3 mi N. Portal, Portal-San Simon Rd.	Cornell Univ. Insect Coll.	2,251	SRR11497540
Neolarra (*Neolarra*) *californica* Michener, 1939 [1]	Mexico, Sonora, Rancho Puerta Blanca	Coll. Minckley, Univ. Rochester	1,180	SRR11497538
Rhopalolemma sp. [2]	USA, AZ, La Paz Co, E Quartzsite	n/a	2,360	SRR11497536
Schwarzia elizabethae Bossert, 2019 [1]	Kenya, Eastern Province, Tsavo East National Park	USNM	2,295	SRR11497535
Schwarzia emmae Eardley, 2009 [1]	Kenya, Rift Valley Province, Mathews Range, Sarara Camp	USNM	2,244	SRR11497534
Schwarzia gretae **sp. nov.** [1]	Kenya, Eastern Province, Ukasi Hill	ICIPE	2,202	SRR11497546
Schwarzia icipensis **sp. nov.** [1]	Kenya, Eastern Province, Ukasi Hill	ICIPE	1,259	SRR11497545
Schwarzia lualenyiensis **sp. nov.** [1]	Kenya, Taita-Taveta County, Lualenyi	National Museums of Kenya	1,569	SRR11497544
Townsendiella pulchra Crawford, 1916 [1]	Mexico, Sonora, 30km E Aqua Prieta	Coll. Minckley, Univ. Rochester	1,938	SRR11497543
Outgroups (generated with Hymenoptera bait set v1, unless otherwise indicated)				
Ericrocis lata (Cresson, 1878)	USA, NM, Hidalgo Co., 4 mi N. Rodeo	n/a	886	SRR5406108†
Hopliphora velutina (Lepeletier & Audinet-Serville, 1825)	Brazil, PR, Porto Amazonas	n/a	1,099	SRR7948343†
Mesonychium jenseni (Friese, 1906)	Argentina, Mendoza, Chacras de Coria	n/a	783	SRR7948345†
Nomada cressonii Robertson, 1893	USA, NY, Tompkins Co., Ithaca	n/a	1,018	SRR7948348†
Oreopasites (*Oreopasites*) *vanduzeei* Cockerell, 1925 (with Hym-v2) [1]	USA, AZ, Cochise Co., 8 km N. Pomerene	Coll. Minckley, Univ. Rochester	1,695	SRR11497537
Paranomada velutina Linsley, 1939	USA, AZ, Cochise Co., Douglas	n/a	1,038	SRR7948347†
Rhathymus bicolor Lepeletier & Audinet-Serville, 1828	Brazil, SP, Luiz Antonio	n/a	891	SRR7948349†
Thyreus delumbatus (Vachal, 1903)	South Africa, NP, 14 km E. Vivo	n/a	1,057	SRR5406026†
Triepeolus verbesinae (Cockerell, 1897)	USA, NM, Hidalgo Co., 4 mi N. Rodeo	n/a	997	SRR7948340†

Scientific names, collection localities, and SRA sequence experiment identifiers for all included samples. Assembled UCE sequence data are available on figshare (Bossert 2020). Superscript numerals indicate in which lab the respective specimens were processed (laboratory 1 or laboratory 2). SRA IDs marked with a dagger (†) are from previously published studies.

with TapeStation, and then size-selected pools showing excessive large fragments to a range of 200–700 bp using the Blue Pippin. Following size selection, libraries were quantified using an Applied Biosystems qPCR instrument with KAPA reagents and pooled at equimolar ratios. Pools from either laboratory were sequenced on Illumina HiSeq platforms with 2 × 150 bp read lengths by Novogene Co., Ltd.

After obtaining the raw reads from the sequencing facilities, FASTQ files were demultiplexed using BBMap (accessed on https://sourceforge.net/projects/bbmap/; see Supp Material [online only]). Adapter sequences were removed with Illumiprocessor (Faircloth 2013), which is a wrapping software around Trimmomatic (Bolger et al. 2014). Adapter removal was assessed with FastQC (Andrews 2019). Reads were assembled with SPAdes (Bankevich et al. 2012) and the MismatchCorrector option. We then used several scripts from the Phyluce pipeline (Faircloth 2016) to match the contig files against the probe set and extract hits as individual UCE sequences. To this end, we used a threshold of 80% sequence identity and overlap. We kept UCE loci with incomplete taxon representation and aligned each locus individually using the L-INS-i mode of MAFFT v7.31 (Katoh and Standley 2013). We then generated a set of UCE loci for which each locus is represented by at least 80% of all taxa (=80% matrix completeness). For this set of loci, we applied an aggressive trimming regime involving three steps. First, we used Gblocks (Castresana 2000) on the individual alignments with the 'relaxed' setting of Talavera and Castresana (2007). We then concatenated the alignments and used Spruceup (Borowiec 2019) to identify and remove windows of outlier sequences. We then split the alignment again per locus (with AMAS; Borowiec 2016) and removed columns from each multiple sequence alignment represented by four or fewer taxa

with trimAl (Capella-Gutiérrez et al. 2009). Finally, we concatenated the resulting 773 individual loci into a supermatrix. Aside from extracting and processing UCE sequences, we searched contigs for COI barcode sequences using the Phyluce script phyluce_assembly_match_contigs_to_barcodes, and uploaded them to the Barcode of Life Data System (Ratnasingham and Hebert 2007). Details on the bioinformatic processing, including the exact program versions and used commands are provided in the Supp Material (online only).

Phylogenetic Reconstruction and Molecular Dating

We calculated a maximum likelihood (ML) tree with IQ-Tree (Nguyen et al. 2015) and designated individual loci as separate partitions. We linked branch lengths over partitions and let the ModelFinder function search for the best-fitting substitution models for each partition (Kalyaanamoorthy et al. 2017). Node support was assessed with 1,000 ultrafast bootstrap approximations (UFBoot2; Hoang et al. 2018).

For divergence time estimates, we reduced the concatenated matrix to 200 selected loci. To this end, we first calculated individual gene trees for all 773 loci with IQ-Tree and assessed the 'clocklikeness' of each individual gene tree using an R script from the repository of Borowiec et al. (2015; see Supp Material [online only]). We ranked loci by their clocklikeness and concatenated the alignments of the corresponding 200 best-performing loci (i.e., those with the lowest variation in root to tip lengths). We then used PartitionFinder2 (Lanfear et al. 2016) to search for the optimal partitioning scheme given the 200 data blocks, and let the program combine similar subsets. We used a greedy scheme, linked subsets and tested for seven substitution models available in BEAST 2 (Bouckaert et al. 2019). Using BEAUti, we assigned substitution models to 19 subsets identified through PartitionFinder2 and let BEAST estimate rate heterogeneity among sites. We linked clock and tree rates over partitions and used a lognormal relaxed molecular clock. We used the single known nomadine fossil *Paleoepeolus micheneri* Dehon, Engel, and Michez, 2017 (Dehon et al. 2017) to inform the divergence time estimates. Geometric morphometric analyses indicate that this fossil belongs to the extant tribe Epeolini Linsley and Michener, 1939 (Dehon et al. 2017), which is represented in our data set by *Triepeolus verbesinae* (Cockerell, 1897). We therefore calibrated the divergence event of this taxon and *Paranomada velutina* Linsley, 1939 with an approximate age of the Menat Formation (i.e., 59.2–56.0 million years ago [mya], from the The Paleobiology Database, 2019). Specifically, we used a log-normal distribution with M = 8.0, S = 1, and an offset of 56.0. We further applied a diffuse prior on the root age of Nomadinae based on previous estimates for this clade (Cardinal and Danforth 2013, Cardinal et al. 2018). To this end, we applied a normal distribution with a mean of 84.0 and σ = 5.5. We used the ML estimate from IQ-Tree as starting tree and let BEAST infer topology and optimize node heights for at least 75 million generations in two separate runs. Convergence was assessed in Tracer (Rambaut et al. 2018) and runs were terminated after the combined ESS of the likelihood exceeded 5,000. We then processed the output trees using the standard programs of the BEAST package. We first combined tree files with LogCombiner and variable burn-ins, and then summarized the trees into a maximum clade credibility tree with median heights using TreeAnnotator.

Biogeographical Analyses and Distribution Maps

To better understand the evolutionary history of *Biastes*, *Townsendiella*, *Schwarzia*, and *Neolarra* through time and space, we estimated potential ancestral ranges for these lineages. We considered three biogeographical divisions: the Afrotropical realm (Af), Nearctic (Ne), and Palearctic (P). We used the fossil-calibrated phylogram from BEAST, pruned the primarily Nearctic outgroup taxa and coded the presence/absence of species in our regions as in Fig. 1. We then used BioGeoBEARS (Matzke 2018) to assess model fit of three models implemented in the maximum likelihood framework of this package: the DEC model (originally developed by Ree and Smith 2008), and the ML adaptations of the DIVA (Ronquist 1997) and BayArea (Landis et al. 2013) models: DIVA-like and BayArea-like (Matzke 2018). We allowed the founder-event speciation parameter (+*j*) and designated a maximum of two possible ranges but excluded the range combination Nearctic + Afrotropics from being considered, given the distance between these areas at the investigated time periods. We further lowered the probability of a direct dispersal between these regions by setting a dispersal multiplier of 0.5, whereas all other combinations were kept at the default of 1. We choose the best-fitting model based on the corrected AIC. Paleogeographical maps used in this study were purchased from Colorado Plateau Geosystems Inc. and are part of their Global Paleogeography series.

Terminology and Documentation

Type specimens from this study are deposited in the collections of the National Museums of Kenya (NMK, holotypes), the International Centre of Insect Physiology and Ecology (ICIPE, paratypes), and the National Museum of Natural History, Smithsonian Institution, Washington, DC (USNM). For the alpha taxonomic descriptions, we used the following abbreviations: tergum (T), sternum (S), and flagellomere (FL). Morphometric measurements are given as a range if more than one specimen was examined. We used SimpleMappr (Shorthouse 2010) to generate a template for the present-day distribution map of *Schwarzia*. All specimens were imaged with a Macropod Pro imaging system and were Z-stacked with Zerene Stacker Pro v1.04.

Morphological Data

As starting point for our assessment of morphological characters, we extracted the matrix of adult and larval characters from Policarová et al. (2019). We then expanded this matrix by coding characters of adult and immature life stages of included taxa that were not part of the original matrix. Characters were primarily obtained through morphological examination, but we also extracted morphological characters of all life stages (adults, mature larvae, first larval instars, egg chorion) from published literature. We used the established character states to guide our diagnoses of the taxa treated herein, but we did not systematically assess the polarity of character states in a cladistic framework. Given the great morphological diversity of Nomadinae and the high potential for morphological convergence due to the shared cleptoparasitic lifestyle, such analyses seem premature for our focused taxon sampling and would require a broader sampling of the subfamily. Our detailed diagnoses of the treated genera comprise all recognized character states and are provided below.

Results

UCE Sequencing

After assembling trimmed Illumina reads with SPAdes, we captured an average of ~1,980 UCEs for newly analyzed samples (Table 1). Combining these with previously published UCE sequence data resulted in an 80% completeness matrix of 773 UCEs, 464,155 bp length, and 25.6% undetermined nucleotide positions. Concatenation of the 200 UCEs that behaved most clocklike in their gene tree estimates resulted in a gappier matrix of 103,639 bp and 34.2% missing data. This matrix was divided into 19 subsets with

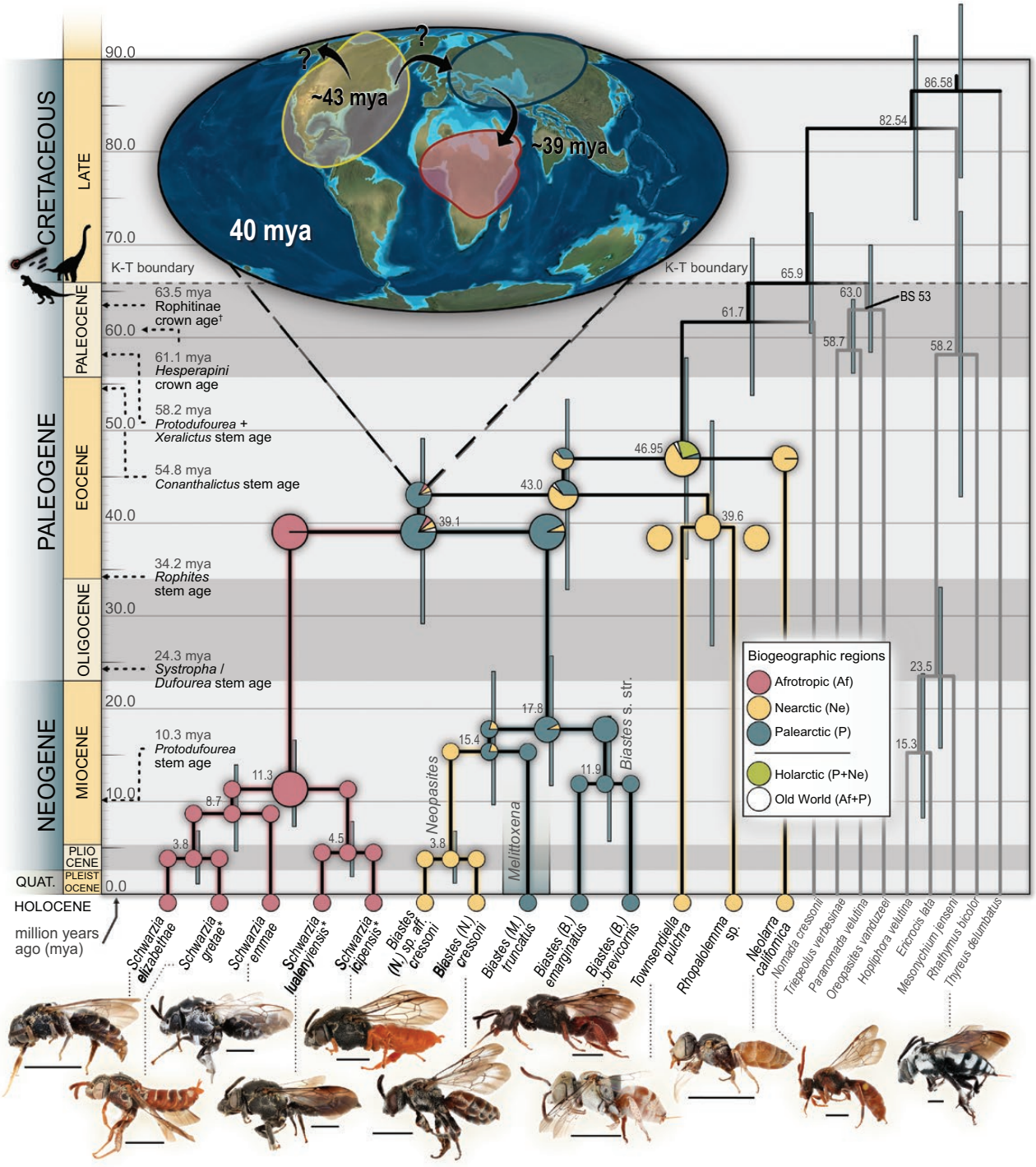

Fig. 1. Fossil-calibrated chronogram of Neolarrini in the new sense (including *Biastes, Neolarra, Rhopalolemma, Townsendiella* and *Schwarzia*) based on 773 ultraconserved elements. Pie charts show possible ancestral ranges. Individual slices are scaled according to their probability as calculated through BioGeoBEARS. Bootstrap support (BS) values and posterior probabilities are omitted but correspond to 100 and 1.0 for all nodes, except for the branching of *Oreopasites* which has a lower BS value. Asterisks (*) indicate newly described species. Stem and crown ages of host taxa along the timeline on the left are taken from Cardinal et al. (2018). Scale bars next to specimen photographs indicate 2 mm length.

separate substitution models as designated by PartitionFinder. We captured 657 bp long COI barcode extracts for all five species of *Schwarzia*, except for *Schwarzia icipensis*, which had 641 bp and 16 ambiguous positions replaced by Ns. COI sequence divergence among these taxa ranged from 4.7% to 8.7% (Table 2).

Phylogeny and Summary of Taxonomic Changes

Both the IQ-Tree and BEAST analyses resulted in a well-supported topology with only the single divergence event of an outgroup taxon, *Oreopasites vanduzeei* Cockerell, 1925, being not supported by the highest possible support values (Fig. 1). The five species of *Schwarzia*

Table 2. COI barcode sequence divergence (K2P) in %

	Schwarzia emmae	*Schwarzia elizabethae*	*Schwarzia gretae*[a]	*Schwarzia icipensis*[a]	*Schwarzia lualenyiensis*[a]
Schwarzia emmae	–				
Schwarzia elizabethae	5.872	–			
Schwarzia gretae[a]	8.734	4.724	–		
Schwarzia icipensis[a]	7.374	6.530	8.078	–	
Schwarzia lualenyiensis[a]	7.028	7.225	7.717	6.179	–

[a]Newly described taxa.

were recovered as monophyletic sister group to a clade comprising *Biastes* and *Neopasites*, thus confirming its presumed close phylogenetic relationship to *Biastes*. *Biastes truncatus* (Nylander, 1848), however, renders *Biastes* paraphyletic in respect to *Neopasites*. Furthermore, the sister group relationship of *Townsendiella* and *Rhopalolemma* shows Biastini to be paraphyletic as used by contemporary classifications (Fig. 2). To solve these issues, we propose a revised classification to maintain a rank-based taxonomy of monophyletic groups. The proposed changes are formally treated below and summarized as follows:

(1) *Biastes*, **stat. rev.** Paraphyly of *Biastes* in respect to *Neopasites* is solved by two taxonomic changes. First, we lower the rank of *Neopasites* and designate it as a subgenus of *Biastes*. This has been suggested previously (Michener 2007) and is further justified by the lack of morphological divergence between the groups. Second, we resurrect *Melittoxena* as a third subgenus of *Biastes* to include *B. truncatus* as well as two other species.

(2) Neolarrini, **stat. rev.** Paraphyly of Biastini is due to the placement of *Rhopalolemma* as sister group to the monogeneric Townsendiellini. This placement has previously been inferred using larval morphological data (e.g., Rozen et al. 1997). Instead of describing another small monogeneric tribe for the genus *Rhopalolemma* with just two species, we designate *Rhopalolemma* and *Townsendiella* to be united in the same tribe. Assessing the morphological diagnosability of this expanded tribal concept revealed an even broader tribal configuration with inclusion of the monogeneric Neolarrini as preferable. While this rearrangement is technically not necessary to maintain monophyletic groups, it is preferable because of a much greater suite of shared morphological characters (Fig. 2), the age of the clade and the reduction of unnecessary monogeneric tribes. We therefore argue that Neolarrini and Biastini should be united in a single tribe. Since Neolarrini has been described before Biastini (Fox (1894) and Linsley and Michener (1939), respectively), Neolarrini receives precedence and Biastini is formally synonymized.

Divergence Time Estimates and Historical Biogeography

According to our BEAST analyses, the tribe Neolarrini in the new sense originated in the early to mid-Paleogene (crown age 57.0–36.2 mya, 95% HPD) around 9–30 mya after the K–T boundary (Fig. 1). *Schwarzia* diverged from the most recent common ancestor (MRCA) with *Biastes* around 40 mya, thus rendering the genus a rather old Afrotropical lineage of cleptoparasites. Crown ages of *Schwarzia* and *Biastes* fall into the mid-Miocene (11.3 and 17.8 mya, respectively). All known host lineages of Neolarrini excluding *Neolarra* (i.e., the former Biastini + *Townsendiella*) originated before their brood parasites based on previously published stem age divergence time estimates (from Cardinal et al. 2018; Fig. 1 herein). The exception is *Protodufourea* Timberlake, 1955, the only documented host of *Rhopalolemma*, which diverged from its sister group *Xeralictus* Cockerell, 1927 more recently (~10 mya, Cardinal et al. 2018). However, the lineage comprising *Protodufourea* and *Xeralictus* is also older than the origin of *Rhopalolemma*.

Assessing model fit with BioGeoBEARS favored the DIVA-like model with founder-event jump dispersal (+*j*) over the DEC and BayArea-like models. According to this analysis, the MRCA of Neolarrini in the new sense was most likely exclusively Nearctic or, with much lower probability, present in Nearctic + Palearctic (Fig. 1). The two earliest branching lineages, *Neolarra* and *Townsendiella* + *Rhopalolemma*, are only found in North America. In the second half of the Eocene (~43 mya, 95% HPD 53.3–32.9), the MRCA of *Schwarzia* + *Biastes* most likely dispersed from North America to the Palearctic. From there, one lineage dispersed shortly thereafter (~39 mya, 95% HPD 49.1–29.2) to the Afrotropical realm, giving rise to present-day *Schwarzia*. The second lineage represents the MRCA of *Biastes*, and the two subgenera *Biastes* s. str. and *Melittoxena* originated in the Palearctic. One lineage of *Biastes*, nowadays represented by the subgenus *Neopasites*, transitioned from the Palearctic to the Nearctic around 15.4 mya (95% HPD 24.0–9.7).

Assessing model fit without the +*j* parameter revealed the DEC model as best-fitting. Estimating ancestral ranges using this model favors an ancestral range of Nearctic + Palearctic for the MRCA of Neolarrini in the new sense and indicated up to seven range-changing events in the lineage that leads up to present-day *Biastes*. The exact estimates for this alternative approach can be found in the Supp Material (online only).

Morphological Characters

We identified diagnostic characters and potentially apomorphic character states for all neolarrine genera. The most important characters are listed in Table 3. Character states that we deem essential for diagnoses of the respective lineages are graphically represented in the summary of phylogenetic relationships (Fig. 2). This graphical representation does not represent cladistic character mapping and does therefore not explicitly distinguish between apomorphic and plesiomorphic character states.

Nomenclature

This paper and the nomenclatural act(s) it contains have been registered in Zoobank (www.zoobank.org), the official register of the International Commission on Zoological Nomenclature. The LSID (Life Science Identifier) number of the publication is: urn:lsid:zoobank.org:pub:29BBF8F7-5468-4432-8717-5782F5A40831.

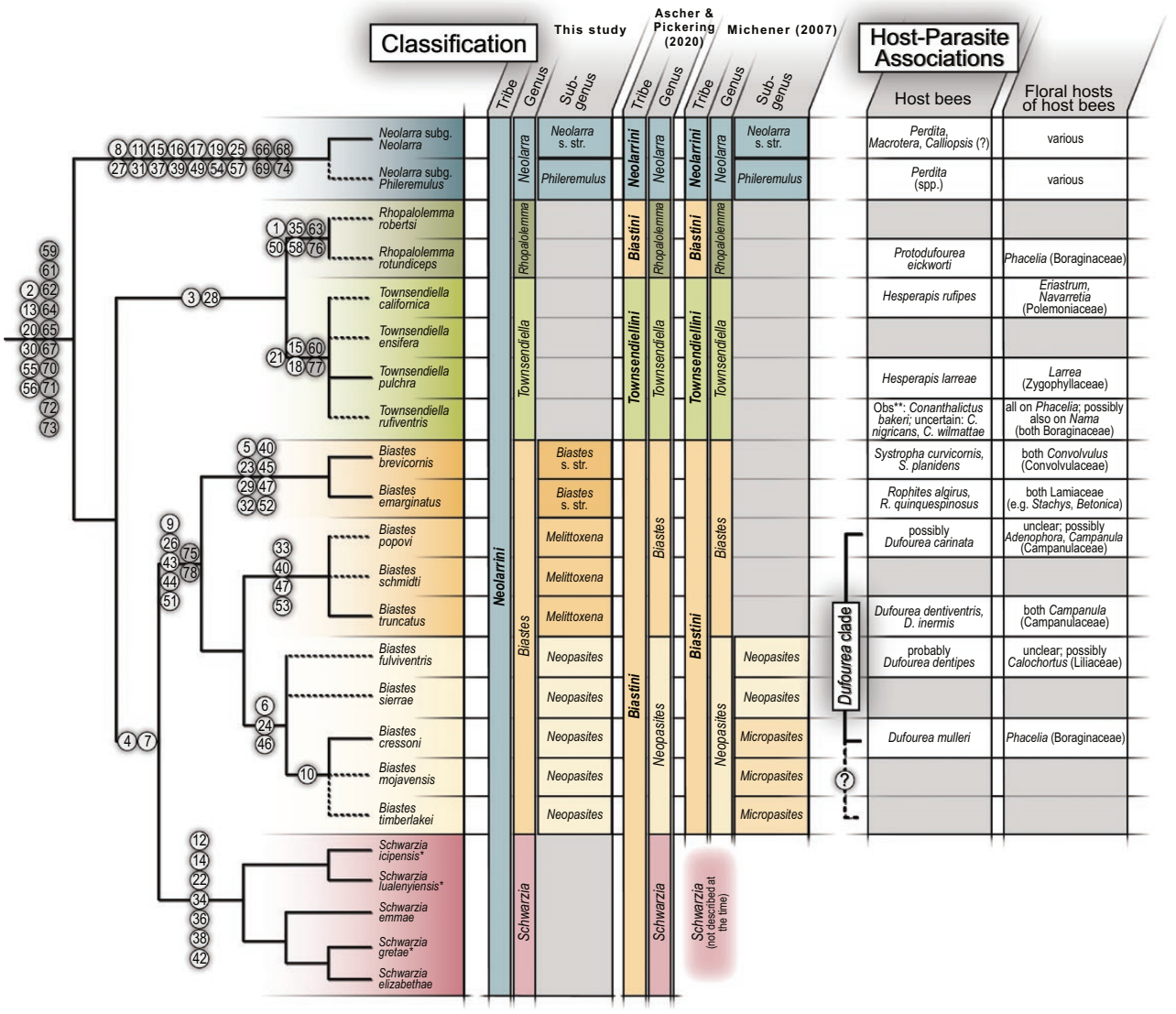

Fig. 2. Summary of phylogenetic relationships of Neolarrini with all described species, except for *Neolarra*. Solid lines show relationships estimated with molecular data and placements with dashed lines are derived from morphology or taxonomic information. Mapped diagnostic characters are listed in Table 3. Larval morphological characters are indicated by a gray background. Information on bee and floral hosts is taken from various sources (Michener 1936, Torchio et al. 1967, Krombein et al. 1979, Warncke 1981, Warncke 1982, Janzon and Svensson 1984, Westrich 1990, Rozen and McGinley 1991, Rozen et al. 1997, Bogusch 2003, Proshchalykin and Lelej 2004, Rozen et al. 2009, Orr and Griswold 2015, Scheuchl and Willner 2016, Westrich 2018). The higher classification of plants follows the APG IV system (The Angiosperm Phylogeny group 2016). Warncke (1982) also lists *Systropha curvicornis* and *S. planidens* as hosts of *Biastes emarginatus* but the source for this information is unclear and has been doubted by other authors (Westrich 2018). No host information is available for *Schwarzia* and species for which boxes are gray. Asterisks (*) indicate newly described species.

Systematics

Neolarrini Fox, 1894: 302.

Type genus: *Neolarra* Ashmead, 1890.

= Biastini Linsley and Michener, 1939: 272. Type genus: *Biastes* Panzer, 1806. **Syn. nov.**

= Neopasitini Linsley and Michener, 1939: 274. Type genus: *Neopasites* Ashmead, 1898. **Syn. nov.**

= Townsendiellini Michener, 1944: 277. Type genus: *Townsendiella* Crawford, 1916. **Syn. nov.**

Diagnostic Characters

Adults: Adult individuals of the tribe Neolarrini in the new sense can be distinguished from other tribes of the subfamily Nomadinae by the following characters. The head is rounded without a paraocular carina along the inner margin of the compound eye. The pedicel is unusually robust and long in comparison to the scape and the first flagellomere. The pedicel is longer than two-fifths and often about half as long as the scape or longer (0.4–0.7× of scape length). It is at most one-third shorter than the first flagellomere, but frequently about as long as, or even much longer (0.7–2.5× of first flagellomere length). In most species of Neolarrini, the propodeal profile has a distinct, nearly horizontal basal zone, behind which it rather abruptly bends down to form the declivous posterior surface. However, this character is strongly reduced to missing in *Rhopalolemma* and *Townsendiella*, and the propodeum in *Schwarzia* may be so short that the character is indistinct. This character is well developed in *Neolarra* and *Biastes* (in the new sense) and is unique within the crown lineage of Nomadinae.

Table 3. Listed are diagnostic and potentially apomorphic character states that are shown on the phylogenetic summary of Neolarrini and included genera in Fig. 2

Number	Character state
1	A: Lateral margin of the clypeus carinate with shiny groove laterally (in female only).
2	A: Pedicel robust and long, about 0.4–0.7× as long as scape and 0.7–2.5× as long as first flagellomere.
3	A: Scape narrow and long in appearance, about 1.75× longer than wide.
4	A: Scape wide and short in appearance, about 1.50× longer than wide.
5	A: Labrum nearly as long as wide.
6	A: Labrum distinctly wider than long, with tooth present.
7	A: Labrum apically straight or nearly so.
8	A: Maxillary lacinia membranous, sclerite missing or largely reduced.
9	A: Maxillary palps with four palpomeres.
10	A: Maxillary palps with one or two palpomeres.
11	A: Base of first palpomere incised on inner margin so that the base appears strongly narrowed.
12	A: Omaulus carinate.
13	A: Propodeal profile with a nearly horizontal basal zone, behind which it rather abruptly turns downward to form the declivous posterior surface.
14	A: Propodeum short with the nearly horizontal basal zone strongly reduced, but tentatively distinct in most specimens.
15	A: Scale-like setae present, often also on propodeal triangle (metapostnotum).
16	A: Forewing venation extends only slightly beyond middle of wing. Large part of wing without venation.
17	A: Marginal cell of forewing about as long as stigma or slightly longer.
18	A: Apex of marginal cell of forewing separated from wing margin, slightly pointed.
19	A: Wing with one or two submarginal cells. Second submarginal cell, if present, very small, only one-third of the first.
20	A: Two submarginal cells in forewing.
21	A: Second submarginal cell of forewing reduced, nearly twice as short as first.
22	A: Second submarginal cell of forewing reduced, twice as short as first.
23	A: Second submarginal cell of forewing distinctly longer than the first.
24	A: Second submarginal cell of forewing slightly shorter than the first.
25	A: First recurrent vein joins first submarginal cell.
26	A: First recurrent vein joins second submarginal cell distant from first submarginal crossvein.
27	A: Front wing largely bare, without vestiture.
28	A: Second segment of foretarsus asymmetrical.
29	A: Hind tibia laterally covered with distinct integumental protuberances bearing minute spines.
30	A: External surface of hindleg metatarsus distinctly flattened, usually more than 1.5× higher than wide in cross section (females).
31	A: Shape of claws normal, convex with pointed, thin teeth on all claws.
32	A: Disc of at least S3–S4 of male medially covered with brushes of long setae.
33	A: S3–S5 of male with fringe of long setae on apical margin.
34	A: S1–S5 with distinct transversal ridge.
35	A: S5 of female tuberculate.
36	A: S5 of female gibbous.
37	A: Apex of S6 of female without specialized coarse setae.
38	A: S6 of female narrowly prolonged with two parallel apical processes.
39	A: T5 of female without pseudopygidial area.
40	A: T5 of female with semicircular pseudopygidial area.
41	A: T5 of female with ill-defined lunule of fine setae suggesting pseudopygidial area.
42	A: T5 of female uniquely modified, with lateral projections bent posteriorly, thereby forming a closed but unpigmented window posterior to pseudopygidial area. Additionally, with an unclosed hole through which S6 protrudes apically.
43	A: Pygidial plate of T6 of female absent.
44	A: T6 modified, emarginated, laterally projecting in angulated corners.
45	A: T6 of female laterally projecting in sharp corners in acute angle; sharply emarginated medially.
46	A: T6 of female laterally projecting in nearly rectangular corners, obtusely emarginated medially.
47	A: Dorsal surface of T6 of female with two large glabrous plates.
48	A: Entire dorsal surfaces of T6 of female covered by setae.
49	A: Pygidial plate on T7 of male absent.
50	A: Female gonostylus clubbed.
51	A: Female gonostylus thickened medially.
52	A: Sting bifid apically.
53	A: Sting pointed apically.
54	A: Male gonobase not evident ventrally (absent or possibly fused to gonocoxites).
55	A: Gonocoxite with septum, represented externally by sulcus, thereby separating basal and apical parts of gonocoxite.
56	A: Ventral parapenial lobe of gonocoxite present, with strong, often peg-like setae.
57	A: Male volsella form a free sclerite, which is not chelate.
58	A: Penis in male with strong basiventral projection.
59	L: Secondary ridge connecting hypostomal ridge and postoccipital ridge (ramus) absent.
60	L: Head capsule wide, parietals so enlarged that the head capsule appears to have a median depression in frontal view.
61	L: Postoccipital ridge ambiguously delimited, appearing doubled.
62	L: Frontoclypeal area, in lateral view rounded, greatly produced.
63	L: The clypeus is strongly recessed so that the labrum is produced slightly beyond the clypeus in lateral view.
64	L: Epipharingeal spiculations absent.
65	L: Labrum only moderately projecting beyond clypeus in lateral view.
66	L: Salivary opening projecting as far as, or farther than hypopharynx in lateral view.
67	L: Apical part of mandible tapering to attenuate.
68	L: Apex of labium with spicules.
69	L: Labium (though short) distinctly produced over maxilla.
70	L: Maxillary palps apparently absent.
71	L: Hypopharinx of normal size, not enlarged.
72	L: Venter of abdominal segment IX distinctly protuberant.
73	L: Venter of abdominal segment X modified, slightly to distinctly produced, or prolonged.
74	L: Abdominal segment X prolonged and anus positioned apically.
75	L: Venter of abdominal segment X distinctly produced.
76	E: Multiple lamellate tubercles present.
77	E: Lamellate tubercles missing.
78	E: Single lamellate tubercle present.

A, adult; L, mature larva; E, egg chorion.

The character states of *Rhopalolemma* and *Townsendiella* are likely reversals and may be related to their mode of parasitism. The profile of the scutellum is frequently convex (even projecting in some species), positioned horizontally, subhorizontally, but also slanting. The metanotum is slanting in most species, but never vertical below the scutellum. The wings usually have two submarginal cells in the forewing, but sometimes just one in *Neolarra* and three in some individuals of *Rhopalolemma*. A septum on the gonocoxite of the male is present and represented externally by a sulcus that separates the basal and apical parts of the gonocoxite. The ventral parapenial lobe of the male gonocoxite is present and bears thick, often peg-like setae. The external surface of the hindleg metatarsus in females is distinctly flattened and usually more than 1.5× higher than wide in cross section. This character is unusual for Nomadinae. However, it is reduced in some species of *Neolarra* and the metatarsus of *Biastes brevicornis* (Panzer, 1798) is thickened in a way that renders this character not applicable. The sixth tergum of females is modified, slightly to strongly emarginated, and with or without distinct lateral corners. Although this character is not developed in all Neolarrini, it is a typical feature of this tribe and likely apomorphic. Tergum 6 is emarginated in most *Neolarra* and without lateral corners. It is not emarginated but with lateral corners in *Rhopalolemma* and *Schwarzia*, and unmodified in *Townsendiella*.

Several of the aforementioned characters are shared with the tribe Hexepeolini Linsley and Michener, 1937, such as the missing paraocular carina and certain features of the male genitalia. Neolarrini differ from Hexepeolini by a series of plesiomorphic characters that are widely distributed in Nomadinae: the transparent margin of the galeal blade forms at least one-third of the galeal width measured midway between the galea base and its apex. The lorum and mentum are fused. The pre-episternal internal ridge (corresponding at least partially to the external pre-episternal groove) is short and not reaching the level of the scrobe. However, the pre-episternal internal ridge is completely absent in *Biastes brevicornis*, the only *Biastes* species studied for this character. The hindleg tibia is without a basitibial plate. The eight sternum of males has a single apical projection with a moderately sized basolateral arm. The sclerotization of the ventral area of sternum 6 in females is weak and membranous medially, often transparent. This character does not apply to females of *Neolarra* and *Schwarzia*, in which the sternum 6 is highly modified and bifid, thus resembling females of Ammobatini Handlirsch, 1925. Lastly, two potentially apomorphic characters are shared in Neolarrini except for *Neolarra* and could represent the ancestral state for this lineage. First, the flabellum is constricted at the base. Second, the internal apophyseal arms of the prosternum are separated. These characters need further study in *Neolarra*, preferably in species with greater overall body size, in order to confirm that these are truly different or just greatly miniaturized.

Mature larvae: Shared morphological features of Neolarrini in the new sense are more distinct in the mature larvae than in adults. Neolarrini differ from all other tribes of Nomadinae by the following set of characters. The epipharynx is smooth and without spiculations. The frontoclypeal area is greatly produced and rounded in lateral view. The labrum is only moderately projecting beyond the clypeus in lateral view. The apical portion of the mandible is narrowly tapering to attenuate. The maxillary palps are apparently absent (cf., Rozen et al. 2009). The venter of abdominal segment X is modified and slightly to distinctly produced or prolonged. The anus is positioned dorsally, except in some species of *Neolarra* and *Biastes* in which it is positioned slightly medially. The postoccipital ridge is diffusely delimited with two faint ridges and thus appears doubled. Three characteristic features of the larva are further shared with *Hexepeolus* Linsley and Michener, 1937. First, the ramus which forms the secondary ridge connecting the hypostomal ridge and the postoccipital ridge is absent. Second, the size of the hypopharynx is reduced and of similar size to those of other nonparasitic apid bee larvae. It is not enlarged as usually the case for larvae of Nomadinae. Third, the venter of abdominal segment IX is distinctly protuberant. In contrast, Neolarrini differ from Hexepeolini in several likely plesiomorphic characters that are common in other Nomadinae. In Neolarrini, the anterior tentorial pit is positioned low in the face and seems clearly closer to the anterior articulation of the mandible than to the antenna. The epipharinx is not produced as a distinct lobe. The apex of the mandible is acute or narrow (and not broadly rounded). The apical mandibular concavity is weakly developed and indistinct, and the labio-maxillary region is strongly recessed.

First instar larvae: The first instar larvae may possess valuable characters for a tribal diagnosis but are only described for *Biastes*, *Neopasites* (Rozen et al. 2009) and *Townsendiella* (Rozen and McGinley 1991). Rozen et al. (2009) anecdotally mention a 'striking resemblance' between the first instar larvae of these bees compared to those of *Neolarra*, but a detailed account on the morphology of this larval stage has never been published for *Neolarra*. They all share a strongly produced elevation on the rear area of the head capsule, followed by an abrupt decline toward the postoccipital ridge. This leads to an essentially straight lateral profile from the base of the clypeus to the highest point of the head capsule (Rozen et al. 2009).

Egg chorion: The egg chorion is either unspecialized with small produced micropyle in *Townsendiella* (Rozen and McGinley 1991), simple eggs in *Neolarra* (Shanks 1978), or with one or multiple lamellate tubercles in the *Biastes* subgenera *Biastes* s. str. and *Neopasites*, as well as in *Rhopalolemma* (Rozen et al. 1997, Rozen and Özbek 2003). Lamellate tubercles are unique among eggs of nomadine bees and may be present in the many species of Neolarrini for which the egg morphology is unknown.

Hosts: Hosts of Neolarrini are predominantly species of Rophitinae (Halictidae) but also Dasypodainae (*Hesperapis* Cockerell, 1898, Melittidae) and Panurginae (Andrenidae) (Fig. 2).

Biastes Panzer, 1806

Type species: *Tiphia brevicornis* Panzer, 1798

Diagnostic Characters

Adults: Species of *Biastes* clearly differ from other genera of Neolarrini in their wing venation and the shape of T6 in females. The first recurrent vein joins the second submarginal cell distant to the first submarginal crossvein. T6 in females is distinctly modified, with a median emargination and laterally projecting, angulated corners (cf. illustrations in Bossert 2019, their Fig. 7; Scheuchl 1995). There is no pygidial plate. The female gonostylus is somewhat thickened medially. Other diagnostic characters are shared with other lineages, particularly with *Schwarzia*, but not in the following unique combination: the mandible has a distinct preapical tooth. The scape is short and wide and about 1.50× longer than broad. The apical margin of the labrum is straight, or nearly so. The lateral expansion of the internal thickening of the integument above the epistomal ridge is reduced and its length is about half the width of the socket diameter (this corresponds to character 16 of Roig-Alsina and Michener 1993). This character, however, is unknown in *Schwarzia*. Setae on meso- and metasoma are plumose, sometimes short, but never

scale-like. The propodeal triangle (metapostnotum) is bare. The apex of the marginal cell of the forewing is rounded and terminates separate from the wing margin. The fifth tergum of females has a distinct pseudopygidial area.

Larvae: Larvae of *Biastes* possess only a single known unique morphological character that is not present in at least one other group of Neolarrini. The venter of the abdominal segment X is distinctly stronger produced than in all other genera of the tribe.

Egg chorion: The three species of *Biastes* for which egg morphology has been studied share the presence of a single lamellate tubercle on the egg chorion.

Hosts: Hosts are exclusively representatives of Rophitinae (Halictidae).

Distribution: Holarctic.

Biastes subg. *Biastes* Panzer, 1806

Type species: *Tiphia brevicornis* Panzer, 1798
= *Biastoides* Schenck, 1874. Type species: *Pasites punctatus* Schenck, 1870
= *Rhineta* Klug, 1807. Type species: *Nomada schottii* Fabricius, 1804

Diagnostic Characters

Adults: The subgenus *Biastes* differs from the other subgenera by their labrum being nearly as long as wide and without a tooth on its exposed surface. The hind tibia is laterally covered with distinct integumental protuberances that bear minute spines (compare to drawings in Scheuchl 1995). The second submarginal cell of the forewing is distinctly longer than the first. The sixth tergum of females projects laterally in sharp corners that end in acute angles. The median emargination is sharp. At least the discs of S3–S4 are medially covered with brushes of long setae (also on S5 in *B. emarginatus* (Schenck, 1870); see drawings in Amiet et al. 2007, Scheuchl 1995) in the male. The semi-circular shape of the pseudopygidial area of T5 in females, as well as the presence of two circular glabrous shiny plates on the basal area of T6 are shared with the subgenus *Melittoxena*. The sting is apically bifid as in the subgenus *Neopasites* (Roig-Alsina 1991).

The morphological differences between the two species that we included in the subgenus *Biastes* are rather large. Males of *B. emarginatus* possess antenna with 10 flagellomeres and those of *B. brevicornis* have 11. The maxillary palps of *B. emarginatus* have three palpomeres and the other species has four. The propodeum of *B. brevicornis* is much shorter in comparison to other species of *Biastes* and resembles the propodeum of *Schwarzia*, which is even shorter.

Hosts: Hosts of *Biastes* subgenus *Biastes* are bees of *Rophites* Spinola, 1808 and *Systropha* Illiger, 1806 (Halictidae: Rophitinae).

Distribution: Palearctic.

Note: The two included species of *Biastes* are morphologically so different that their separation into different subgenera could be justified as suggested by Popov (1933). However, using monotypic subgenera with two most closely related species (Fig. 1) does not provide any practical benefit and is therefore omitted.

Species included:
Biastes (*Biastes*) *brevicornis* (Panzer, 1798)
Biastes (*Biastes*) *emarginatus* (Schenck, 1870)

Biastes subg. *Melittoxena* Morawitz, 1873

Type species: *Nomada truncata* Nylander, 1848

Diagnostic Characters

Adults: The morphology of bees of *Melittoxena* is very similar to those of *Neopasites*. They share the specific shape of the labrum: it is distinctly wider than long and has a single median tooth. The hind tibia is laterally covered with spines but without distinct integumental protuberances (compare with drawings in Scheuchl 1995). The second submarginal cell of the forewing is distinctly shorter than the first. Tergum 6 is laterally projecting in nearly rectangular corners (angle of 70–80°) and is obtusely emarginated medially. The maxillary palps have four palpomeres and the antenna in males has 10 flagellomeres in all species. A unique character of the subgenus *Melittoxena* is the arrangement of setae on S3–S5 in males. While there are distinct fringes of long setae on the apical margins of S3–S5, there are dense, short, velvety setae on the discs of these segments. According to Roig-Alsina (1991), the sting is apically pointed, which is unique for *Biastes*. The shape of the pseudopygidial area on T5 in females and the two circular glabrous shiny plates on T6 are as in the subgenus *Biastes*.

The larval stages and the morphology of the egg chorion are unknown.

Hosts: Genus *Dufourea* Lepeletier, 1841 (Halictidae: Rophitinae).

Distribution: Palearctic.

Note: *Biastes schmidti* was associated with the subgenus *Melittoxena* based on the original description (Heinrich 1977).

Species included:
Biastes (*Melittoxena*) *popovi* Proshchalykin and Lelej, 2004
Biastes (*Melittoxena*) *schmidti* Heinrich, 1977
Biastes (*Melittoxena*) *truncatus* (Nylander, 1848)

Biastes subg. *Neopasites* Ashmead, 1898

Type species: *Phileremus fulviventris* Cresson, 1878
= *Micropasites* Linsley, 1942. Type species: *Neopasites cressoni* Crawford, 1916. **Syn. nov.**

Diagnostic Characters

Adults: The subgenera *Neopasites* and *Melittoxena* are very similar in their adult morphology. Bees of both groups have a labrum which is distinctly wider than long and which has a single median tooth. The hind tibia is laterally covered with spines but without distinct integumental protuberances. The second submarginal cell of the forewing is distinctly shorter than the first. Tergum 6 is laterally projecting in nearly rectangular corners (angle of 70–80°) and is obtusely emarginated medially. Males have antennae with only 10 flagellomeres in all species. The maxillary palps have four palpomeres, except in the two species that were formerly placed in the subgenus *Micropasites* (Fig. 2). In these species, the maxillary palps are reduced to two (*Biastes* (*N.*) *cressoni*) or a single palpomere (*Biastes* (*N.*) *fulviventris* (Cresson, 1878), *Biastes* (*N.*) *mojavensis* (Linsley, 1943)). The subgenus *Neopasites* differs from *Melittoxena* as follows. The sting is apically bifid as in the subgenus *Biastes* (Roig-Alsina 1991). The pseudopygidial area of T5 is characteristically reduced to an ill-defined lunule of fine setae, and the entire dorsal surface of T6 is covered by setae, without any glabrous areas as in *Melittoxena*.

Hosts: *Dufourea* (Halictidae: Rophitinae) (Torchio et al. 1967).

Distribution: Nearctic.

Note: The sole significant difference between *Neopasites* s. str. and *Micropasites* is the reduced number of palpomeres in *Micropasites*. While monophyly of *Micropasites* is likely, it is unclear if *Neopasites* in the strict sense is monophyletic. We therefore synonymize these two subgenera in order to avoid a potentially paraphyletic *Neopasites* s. str.

Species included:
Biastes (*Neopasites*) *cressoni* Crawford, 1916, **comb. nov.**
Biastes (*Neopasites*) *fulviventris* (Cresson, 1878), **comb. nov.**
Biastes (*Neopasites*) *mojavensis* (Linsley, 1943), **comb. nov.**
Biastes (*Neopasites*) *sierrae* (Linsley, 1943), **comb. nov.**
Biastes (*Neopasites*) *timberlakei* (Linsley, 1943), **comb. nov.**

Neolarra Ashmead, 1890

Type species: *Neolarra pruinosa* Ashmead, 1890

Diagnostic Characters

Adults: The genus *Neolarra* differs from all other genera by a suite of morphological characters, several of which are likely connected to their minute body size. Most strikingly is the morphology of the wings, which has two or only a single submarginal cell in the forewing. The forewing is largely bare, without vestiture, and the entire venation extends only slightly behind the middle of the wing. The marginal cell is about as long as the stigma or just slightly longer, and the second submarginal cell, if present, is very short and only as long as one-third of the first submarginal cell's length. The first recurrent vein joins the first submarginal cell. The maxillary lacinia of *Neolarra* is membranous and the sclerite is missing or largely reduced. The basal area of the first palpomere of the labial palps is incised on the inner margin, so that the base appears strongly narrowed. The glossa bears a flabellum-like structure but is not constricted at its base. The mandible is simple and without a preapical tooth. The apophyseal arms of the prosternum are fused along the median crest. S6 is strongly modified, narrowed and often bifid. S6 lacks any specialized coarse setae that are present in other Neolarrini. T5 of females do not bear a pseudopygidial area, but the segment is notched or cleft midapically in some species (Michener 1939). The pygidial plate of T6 in females is well developed and is apically emarginated in some species (Michener 1939, Shanks 1978). No pygidial plate is present on T7 of males. The gonobase of males is not evident ventrally and seems either absent or possibly fused to the gonocoxites. The volsella forms a free sclerite which is not chelate and distinctly separate from the gonocoxite. The shape of the claws is normal, thus convex with pointed, thin teeth on all claws. Specimens of *Neolarra* are typically densely covered in thick, scale-like setae, which are also present on the propodeal triangle (metapostnotum).

Larvae: The mature larvae of *Neolarra* differ from those of other members of the tribe in several characters. The salivary opening is projecting as far as, or farther than the hypopharynx in lateral view (Rozen 2001). The labium, which is rather short, is distinctly produced over the maxilla and its apex bears spicules (Rozen 2001). The abdominal segment X is prolonged and the anus is positioned apically.

Hosts: Bees of the genera *Perdita* Smith, 1853 (Andrenidae: Panurginae). Reports for *Calliopsis* Smith, 1853 and *Macrotera* Smith, 1853 (Shanks 1978) are discussed below.

Distribution: Nearctic.

Neolarra subg. *Neolarra* Ashmead, 1890

Type species: *Neolarra pruinosa* Ashmaed, 1890

Diagnostic Characters

Adults: The subgenus *Neolarra* differs from the subgenus *Phileremulus* Cockerell, 1895 in two characters. First, the nominotypical subgenus has the greatest width of the scutellum at or in front of the middle of the scutellum (see also Michener 2007). Second, the outer margin of the axilla is rounded. The venation of the forewing is variable.

Species included:
Neolarra (*Neolarra*) *alba* Cockerell, 1916
Neolarra (*Neolarra*) *batrae* Shanks, 1978
Neolarra (*Neolarra*) *californica* Michener, 1939
Neolarra (*Neolarra*) *clavigera* Shanks, 1978
Neolarra (*Neolarra*) *hurdi* Shanks, 1978
Neolarra (*Neolarra*) *linsleyi* Michener, 1939
Neolarra (*Neolarra*) *orbiculata* Shanks, 1978
Neolarra (*Neolarra*) *penicula* Shanks, 1978
Neolarra (*Neolarra*) *pruinosa* Ashmead, 1890
Neolarra (*Neolarra*) *vandykei* Michener, 1939
Neolarra (*Neolarra*) *verbesinae* (Cockerell, 1895)

Neolarra subg. *Phileremulus* Cockerell, 1895

Type species: *Phileremulus vigilans* Cockerell, 1895

Diagnostic Characters

Adults: The subgenus *Phileremulus* has the scutellum diverging posterior to its greatest width behind the middle of the scutellum and the outer margin of the axilla is produced to an acute tooth (Michener 1939, Shanks 1978, Michener 2007). The forewing has only one submarignal cell in all species and the second recurrent vein is missing.

Note: The morphological differences between the subgenera *Neolarra* s. str. and *Phileremulus* are rather subtle and *Neolarra* s. str. lacks clear apomorphic characters. However, adopting the subgeneric classification of the revisionary treatments which recognize two subgenera (Michener 1939, Shanks 1978) facilitates the usage of published keys and ultimately species identification. Until future phylogenetic research with comprehensive taxon sampling validates or rejects monophyly of these groups, we recognize both subgenera for practical reasons.

Species included:
Neolarra (*Phileremulus*) *alexanderi* Griswold and Parker, 1999
Neolarra (*Phileremulus*) *cockerelli* (Crawford, 1916)
Neolarra (*Phileremulus*) *rozeni* Shanks, 1978
Neolarra (*Phileremulus*) *ute* Griswold and Parker, 1999
Neolarra (*Phileremulus*) *vigilans* (Cockerell, 1895)

Rhopalolemma Roig-Alsina, 1991

Type species: *Rhopalolemma robertsi* Roig-Alsina, 1991

Diagnostic Characters

Adults: *Rhopalolemma* differs from all other genera of Neolarrini in four unique characters. The lateral margin of the clypeus in females is carinate and with a shiny groove laterally (Roig-Alsina 1991, Rozen et al. 1997). The fifth sternum of females is tuberculate (Roig-Alsina 1991). The gonostylus of the sting apparatus is clubbed (Roig-Alsina 1991) and the penis in males has a

well-developed basiventral projection. *Rhopalolemma* is the only genus of Neolarrini in which individual specimens have three submarginal cells in the forewing; however, there seems to be great variation within populations and individuals with two submarginal cells seem to be more common. Certain characters that *Rhopalolemma* shares with *Townsendiella* are different from other Neolarrini: the second tarsomere of the foreleg is distinctly projecting medially and thus asymmetrical (Roig-Alsina 1991, Rozen et al. 1997). The tarsus in *Rhopalolemma* is projecting stronger than in *Townsendiella* and bears a brush of setae on the inner apex (Rozen et al. 1997). The antennal scape is more slender in *Townsendiella* and *Rhopalolemma* than in other genera of Neolarrini and about 1.75× longer than wide. A pygidial plate with carinate margins is present on terminal terga of both sexes of both genera. In other genera which have pygidial plates, they are only present in one sex but not in both. Other characters that differentiate *Rhopalolemma* from the other neolarrine genera are as follows: the mandible is simple and without a preapical tooth. The labrum is broader than long and the apical margin is rounded. The apex of the marginal cell of the forewing is rounded and terminates separate from the wing margin. The first recurrent vein joins the second submarginal cell close to the first submarginal crossvein or is interstitial. The fifth tergum bears a narrow pseudopygidial area.

Larvae: The most striking character of the mature larva of *Rhopalolemma* is the strongly recessed clypeus, which renders the labrum projecting beyond the clypeus in lateral view (Rozen et al. 1997).

Egg chorion: Eggs of *Rhopalolemma* are unique in having multiple lamellate tubercles and are illustrated in detail in Rozen et al. (1997).

Hosts: *Protodufourea eickworti* Bohart and Griswold, 1996 is host to *Rhopalolemma rotundiceps* (Rozen et al. 1997).

Distribution: Nearctic.

Species included:
Rhopalolemma robertsi Roig-Alsina, 1991
Rhopalolemma rotundiceps Roig-Alsina, 1997

Schwarzia Eardley, 2009

Type species: *Schwarzia emmae* Eardley, 2009
Currently known distribution: Fig. 3
Habitat photographs: Fig. 4

Diagnostic Characters

Adults: *Schwarzia* is primarily characterized by the highly modified fifth tergum of the females. T5 has lateral projections that extend posteriorly and form a closed, translucent, unpigmented window posterior to the modified pseudopygidial area (e.g., Figs. 5E and 7D). The projections are further bent in a way that forms a nearly closed hole through which S6 protrudes. T6 of females is hidden under T5, but has a reduced, pygidium-like structure with distinct lateral projections that extend ventrolaterally. The sixth sternum of females is narrow and prolonged, and with two hooked parallel processes apically. These apical processes bear a few coarse,

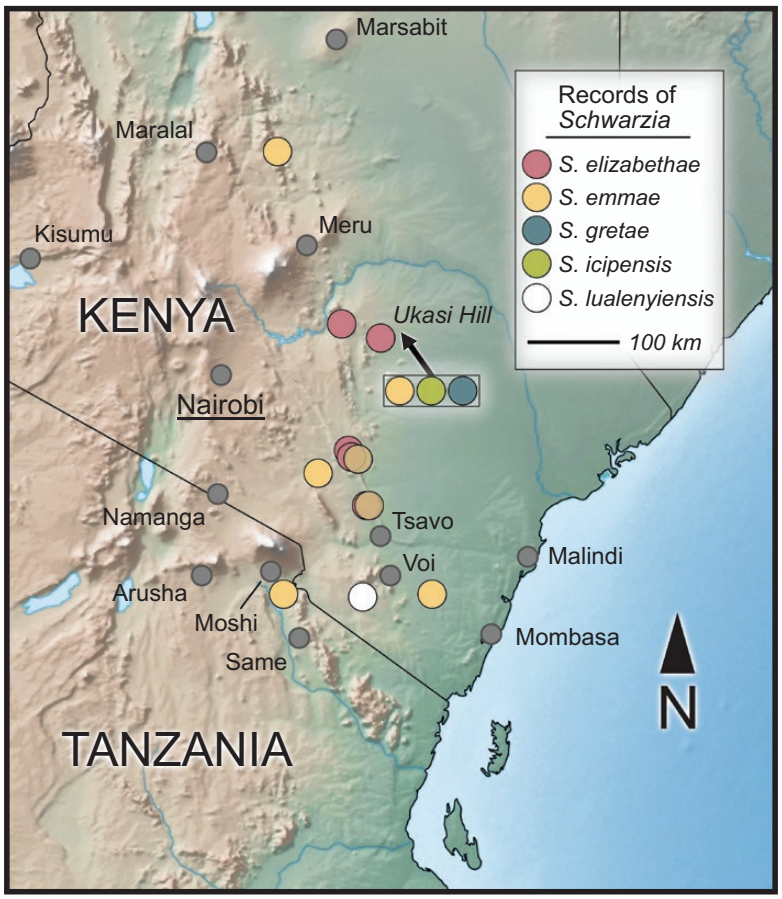

Fig. 3. Distribution map of all currently known records of *Schwarzia*, including the localities from Eardley (2009). Four out of five species were collected in the vicinity of Ukasi Hill.

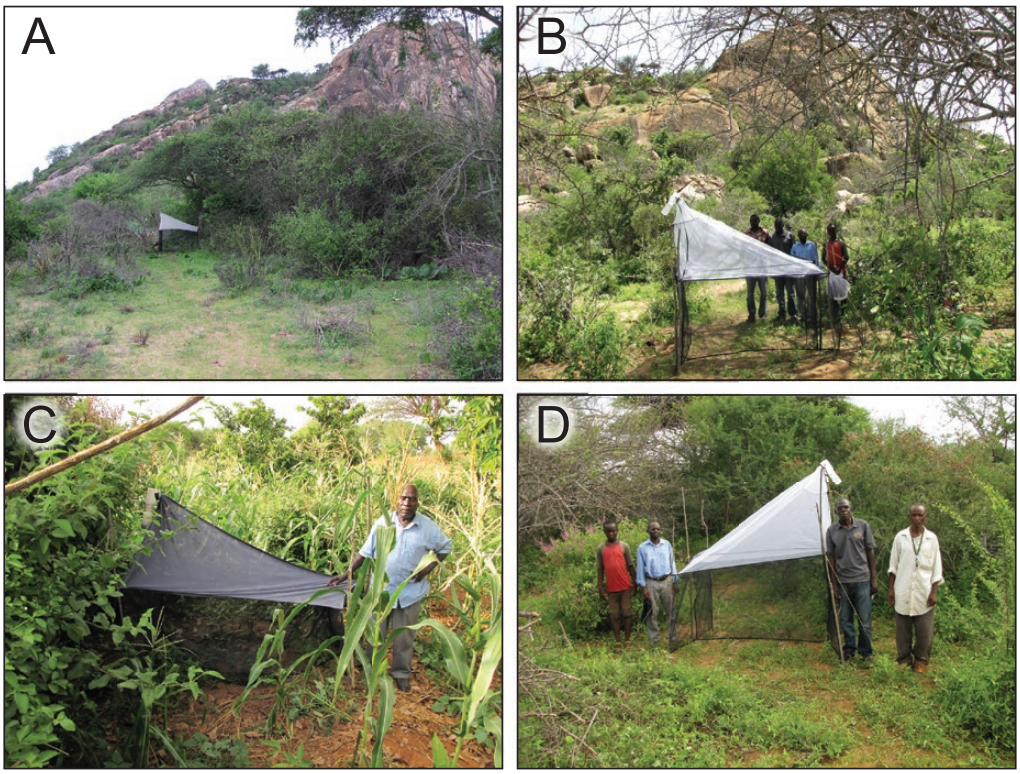

Fig. 4. Habitat photographs of *Schwarzia* collecting sites in Kenya. (A) Ukasi Hill, November 2011. Specimens of *S. elizabethae* and paratypes of *S. gretae* and *S. icipensis* were collected in the area during this month. (B) Ukasi Hill, April 2018. The holotype and paratypes of *S. gretae* were collected near the Hill in April and May. Pictured from left to right are field worker Ken Katinga Ngalu, technical assistant Josephat Bukhebi, technician Joseph Gitau Ndungu, and field worker Richard Maithyia Munyao. (C) Mulu Musingila's farm in Kitui Co. near Tsavo East National Park. Standing next to the trap is farm owner and field worker Mulu Musingila. *Schwarzia elizabethae* and *S. emmae* were collected on the farm in a Malaise trap (December 2016). (D) Sosoma area, April 2018. Habitat of *S. emma*. Pictured from left to right are field worker Richard Maithyia Munyao. Technician Joseph Gitau Ndungu, Technical assistant Josephat Bukhebi and field worker Mung'atu Kimanzi Mwanzau.

downwardly bent setae close to the tip. The sterna preceding S5 are distinctly gibbously shaped in the female. The unmodified sterna are coarsely punctate and have distinct transverse ridges from side to side in both sexes. *Schwarzia* further has a characteristic wing venation in the forewing. The second submarginal cell of the forewing is small, always shorter than half the size of the first submarginal cell. The propodeum is very short and appears declivous. The nearly horizontal basal zone is strongly reduced, but visible and distinct in the larger species of the genus. One species (*S. emmae*) has a small preapical tooth on the mandible but it is lacking in the other species. There may be a slight elevation on the inner margin of the mandible; however, it is not comparable to the truly bidentate mandibles of *Biastes*. The scape is short and thick, and about 1.5× longer than wide, thus similar to *Biastes*. *Biastes* and *Schwarzia* further share the straight apical margin of the labrum. The labrum is broader than long. *Schwarzia* is the only genus of Neolarrini with a lamellate omaulus.

Larval stages and egg chorion of *Schwarzia* are unknown.

Species included:
Schwarzia elizabethae Bossert, 2019
Schwarzia emmae Eardley, 2009
Schwarzia gretae Bossert, **sp. nov.**
Schwarzia icipensis Bossert, **sp. nov.**
Schwarzia lualenyiensis Bossert, **sp. nov.**

Schwarzia elizabethae Bossert, 2019

***Habitat photographs*:** Fig. 4A and C

Material Examined

Type material: HOLOTYPE: KENYA: Eastern Province, at Athi River, Tsavo East National Park, 2°38.51′ S, 38°21.98′ E, 22.–29.XI.1999, leg. R. Copeland, Malaise trap, ♂, dep. NMK. PARATYPES: Eastern Province, at Athi River, Tsavo East National Park, 2°38.51′ S, 38°21.98′ E, 22.–29.XI.1999, leg. R. Copeland, Malaise trap, 4♂, 1♀. Eastern Province, at Athi River, Tsavo East National Park, 2°38.51′ S, 38°21.98′ E, 29.III–1.IV.1999, leg. R. Copeland, Malaise trap, 1♂.

Additional material: KENYA: Eastern Province, base of Ukasi Hill, 0°49.262′S, 38°32.666′E, 21.XI.–05.XII.2011, leg. R. Copeland, Malaise trap, *Acacia*/*Commiphora* savanna, 1♀. Eastern Province, base of Ukasi Hill, 0.82002°S, 38.54378°E, 615 m, 5.–12.V.2018, leg. R. Copeland, Malaise trap, *Acacia*/*Commiphora* savanna, 1♂. Eastern Province, Mulu Musingila's farm, 2.11412°S, 38.23989°E, 689m, 13.–27.XII.2016, leg. R. Copeland, Malaise trap, farmland near small seasonally wet area, 1♂. Eastern Province, Kasaala area, 2.07836°S, 38.22517°E, 16.–30.VI.2018, 733 m, leg. R. Copeland, Malaise trap, inside isolated woodland patch, 1♀. KENYA: Eastern Province, Kamuwongo area, Njeru Ranch, 0.69087°S, 38.07785°E, 7.XI–21.XI.2019, leg. R. Copeland, Malaise trap, degraded shrubland, 1♀. All additional specimens are deposited in the ICIPE collection, Nairobi, Kenya.

Remarks

COI sequence data from this species can be found under process ID SCHW001–19 in the Barcode of Life Data System.

Schwarzia emmae Eardley, 2009

Habitat photographs: Fig. 4C and D

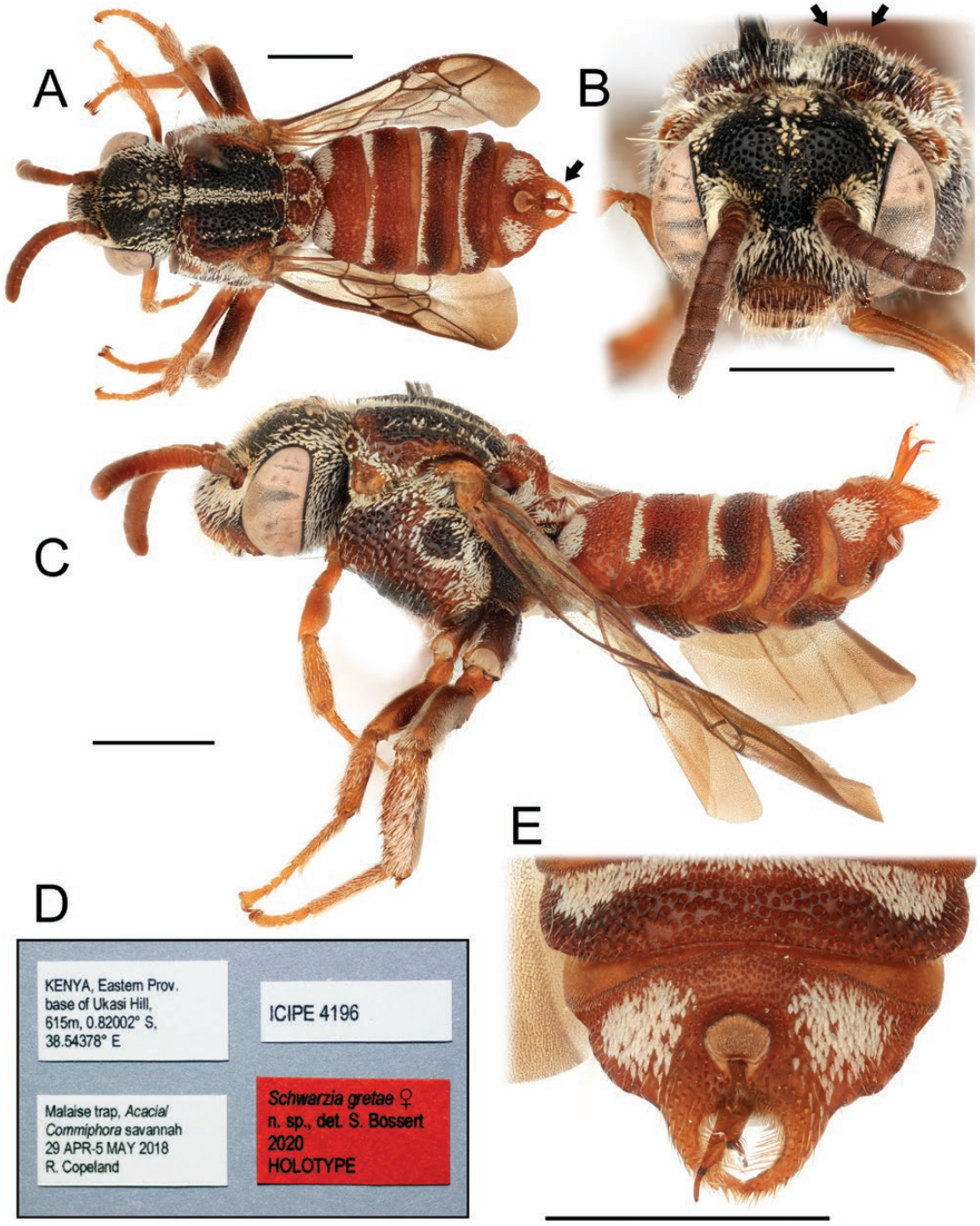

Fig. 5. Female holotype of *Schwarzia gretae* **sp. nov.** (A) Habitus, dorsal view. (B) Habitus, frontal view. (C) Habitus, lateral view. (D) Label information as deposited with the holotype. (E) Details of T4–T5. Scale bars show 1 mm.

Material Examined

KENYA: Rift Valley Province, Mathews Range, Sarara Camp, 1.1°N, 37.387°E, 10.–13.VI.1998, leg. R. Copeland, Malaise trap, 1♂, 1♀, dep. in USNM. Eastern Province, near Athi River, Tsavo East National Park, 2°37′ S, 38°22′ E, 1065 m, 10.VI.1998, leg. R. Copeland, Malaise trap, 1♂, 1♀, dep. in USNM. KENYA: Eastern Province, Sosoma area, 0.86344°S, 38.67907°E, 489 m, 15–29.IV.2018, leg. R. Copeland, Malaise trap, Acacia/Commiphora woodland, 1♀, dep. ICIPE. Eastern Province, Mulu Musingila's farm, 2.11412°S, 38.23989°E, 689 m, 13.–27.XII.2016, leg. R. Copeland, Malaise trap, farmland near small seasonally wet area, 1♀, dep. ICIPE.

Remarks

COI sequence data from this species can be found under process ID SCHW002–19 in the Barcode of Life Data System.

Schwarzia gretae Bossert, **sp. nov.**

Figures 5–6, 10B and D, and 11A

Habitat Photographs: Fig. 4A and B

(urn:lsid:zoobank.org:act:CAAB4791-07D8-4415-A66D-F87A4B3AA1B9)

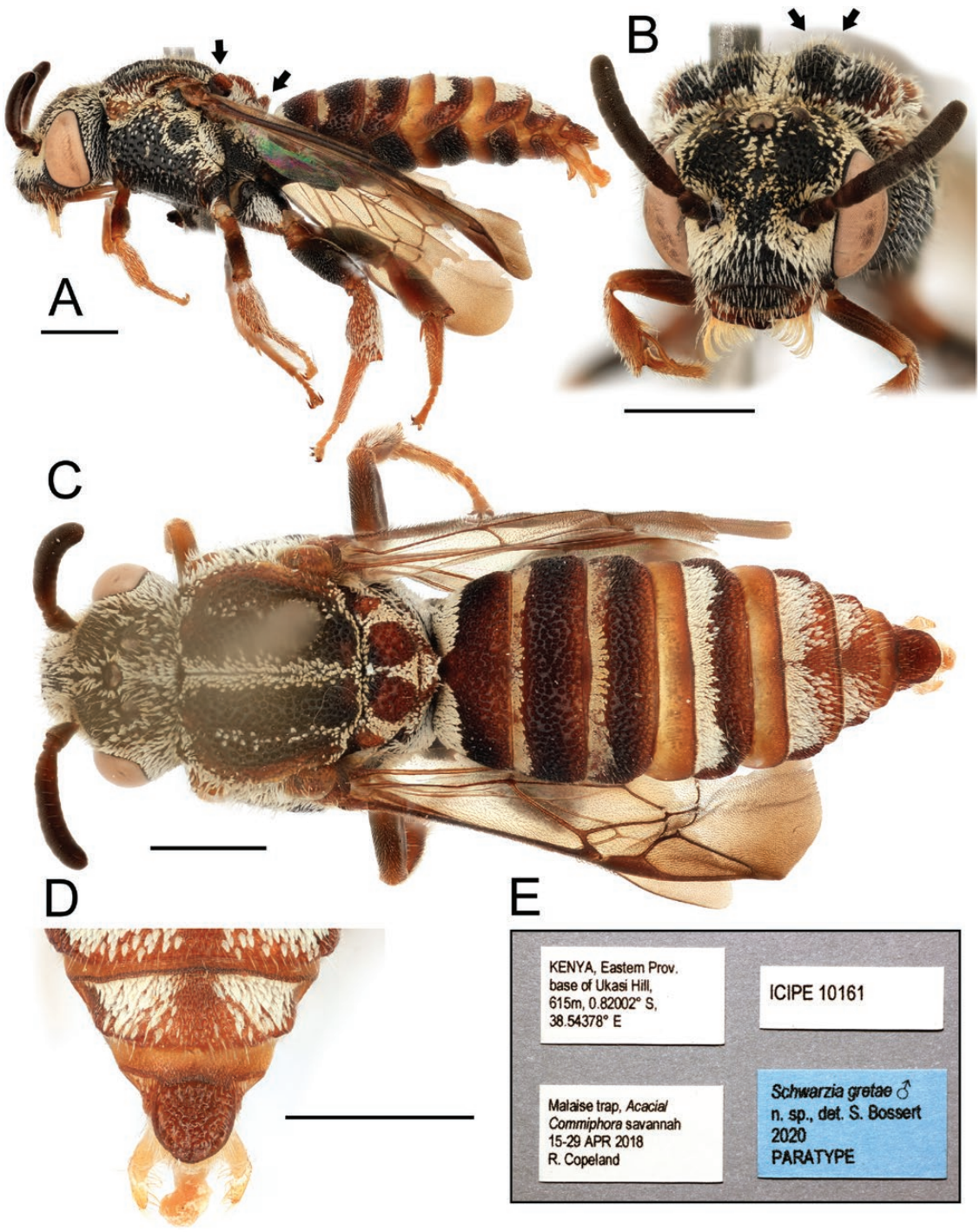

Fig. 6. Male paratype of *Schwarzia gretae* **sp. nov.** (A) Habitus, lateral view. Left arrow points to the lamellate axilla. Right arrow points to the produced, dorsally protruding metanotum. (B) Habitus, frontal view. Arrows point to produced ridges along the mesoscutellar line. (C) Habitus, dorsal view. (D) Details of T6–T7. (E) Label information as deposited with the paratype. Scale bars show 1 mm.

Material Examined

HOLOTYPE: KENYA: Eastern Province, base of Ukasi Hill, 0.82002°S, 38.54378°E, 615 m, 29.IV.–5.V.2018, leg. R. Copeland, Malaise trap, *Acacia*/*Commiphora* savanna, ♀, ICIPE identifier #4196, dep. NMK. Labels of the holotype are shown in Fig. 5D.

PARATYPES: KENYA: Eastern Province, base of Ukasi Hill, 0.82103°S, 38.54443°E, 613 m, 21.XI–5.XII.2011, leg. R. Copeland, Malaise trap, *Acacia*/*Commiphora* savanna, 1♀, dep. ICIPE. Eastern Province, base of Ukasi Hill, 0.82002°S, 38.54378°E, 615 m, 12.–19.V.2018, leg. R. Copeland, Malaise trap, *Acacia*/*Commiphora* savanna, 1♀, dep. ICIPE. Eastern Province, base of Ukasi Hill, 0.82002°S, 38.54378°E, 615 m, 15.–29.IV.2018, leg. R. Copeland, Malaise trap, *Acacia*/*Commiphora* savanna, 1♂ (ICIPE identifier #10161), 1♀, dep. coll. Bossert. Eastern Province, base of Ukasi Hill, 0.82002°S, 38.54378°E, 615 m, 5.–12.V.2018, leg. R. Copeland, Malaise trap, *Acacia*/*Commiphora* savanna, 1♂, dep. ICIPE. KENYA:

Eastern Province, base of Ukasi Hill, 0.82002°S, 38.54378°E, 615 m, 20.XI–4.XII.2019, leg. R. Copeland, Malaise trap, *Acacia*/*Commiphora* savanna, 2♀, 2♂. KENYA: Eastern Province, north side of Ukasi Hill, 0.81529°S, 38.54301°E, 643m, 20.XI–4.XII.2019, leg. R. Copeland, Malaise trap, *Acacia*/*Commiphora* savanna, 1♂.

Diagnosis

Body size 6.7–7.5 mm in male, 6.1–6.9 mm in female. *Schwarzia gretae* is morphologically most similar to *S. elizabethae* and the following characteristics are shared between the two species. No protrusions are present on the supra-antennal area (present in *S. emmae*) and the area is evenly punctate (Fig. 10B). The margin of the compound eye is entire, not indented as in *S. emmae* (cf., Fig. 10A). The punctation on T1 and T2 is coarse and not fine as in *S. emmae* and *S. icipensis* (Fig. 10C and D). The antenna in males has 10 flagellomeres, not 11 as in *S. icipensis* and *S. lualenyiensis*. The pygidial plate of males is shield-shaped (Fig. 6D) and not squared as in *S. lualenyiensis*. *Schwarzia gretae* differs from *S. elizabethae* as follows. Significant portions of the entire integument are reddish-orange (Figs. 5 and 6). The terminal opening on T5 of the females is evenly rounded, with thinner posterolateral projections (Fig. 5E). It is not teardrop-shaped and with thick projections as in *S. elizabethae* (Bossert 2019, their Fig. 3A). The metanotum in *S. gretae* is dorsally projecting (Fig. 11A), stronger than in *S. elizabethae*. The axillae are produced and lamellate (Fig. 11A), and not flat as in *S. emmae*, *S. icipensis*, and *S. lualenyiensis*. The axillae in *S. elizabethae* are more weakly produced than in *S. gretae*. The scutum has two elevated parallel ridges adjacent to mesoscutellar line in both sexes (Figs. 5B and 6B), which are absent in any other known species of *Schwarzia*.

Description

Female (Fig. 5). Head: Head (Fig. 5B) wider than long (1.7–1.9 mm width to 1.2–1.4 mm length). Integument black except labrum and mandible brown. Thick short setae around antennal sockets, along frontal line, median ocellus, genal area (Fig. 10B). Clypeus protruding, much shorter than broad (0.9- to 1.0-mm width to 0.3- to 0.4-mm length). Punctation on clypeus coarse, denser than on supra-antennal area. Mandible brown with darkened tip, unidentate, setae short and sparse. Pre-apical teeth absent. Labrum broader than long. Proboscis short. Width of compound eye about 1.9× the width of genal area in lateral view (Fig. 5C). Deep, pit-like punctation more or less evenly distributed on supraclypeal area, supra-antennal area, frons, vertex; most dense right above antennal sockets (Fig. 5B). Interspaces shiny, granulose protrusions absent. Flagellum with 10 flagellomeres. FL1 broader than long, 0.15- to 0.17-mm width and 0.10- to 0.12-mm length. Both FL2 (0.17- to 0.20-mm width to 0.08- to 0.10-mm length) and FL3 (0.19- to 0.21-mm width to 0.09- to 0.11-mm length) about twice as broad as long (Fig. 5B). Last flagellomere slightly longer than broad: 0.19- to 0.22-mm width to 0.21- to 0.23-mm length. Scape 0.19- to 0.21-mm long. Coloration brown. Diameter of lateral ocellus 0.14–0.16 mm, median ocellus 0.16–0.18 mm. Ocellocular distance 0.39–0.44 mm. Mesosoma: Integument black with extensive red markings along borders of scutum, pronotal lobe, scutellum, axilla, metanotum, tegula, mesepisternum (Fig. 5A and C). Short-thick setae primarily present on margins of segments, i.e., along episternal groove, scrobal groove, around pronotal lobe, posterior margin of scutum, around scutellum, along midline of scutum and parapsidal lines, on metanotum and metapostnotum. Intertegular distance 1.3–1.6 mm. Axillae weakly produced but distinctly lamellate (Fig. 11A). Metanotum dorsally protruding (Fig. 11A). Punctation on scutum deep, irregular, rugose. Pit diameter markedly greater and punctation more rugose than on vertex. Scutum with two elevated parallel ridges adjacent to mesoscutellar line (Fig. 5B). Omaulus lamellate. Punctation on scutellum as on scutum. Wing venation brown. Meso- and metatibial spurs with two ventrally oriented rows of teeth, most strongly produced on metatibia. Metasoma: Integument primarily reddish orange. Basal areas of T2–T4 darkened. T1 with basal patch of thick white setae. T2–T4 with basal bands of setae, T5 with two lateral patches (Fig. 5A). Punctation on T1–T4 coarse, interspaces smaller than pit diameters (Fig. 5A). Punctation on T5 finer than on preceding terga. Disc of T5 with pseudopygidial plate which is slightly broader than long. Posterior T5 with two hook-shaped projections medio-laterally, which form genus-specific opening through which bifid S6 protrudes. Hook-shaped projections thin and opening particularly wide. Punctation on basal areas of S2–S5 very fine and tesselate, distinctly different from coarser punctation medially and posteriorly. Basal areas with lighter integument. Surface of S5 with large shiny area without punctation. S1–S5 without any setae.

Male (Fig. 6). Overall similar to female except terminal terga and slightly darker coloration. Head: Head (Fig. 6B) wider than long (width 1.8–1.9 mm, length 1.2–1.3 mm). Integument black with thick short setae around antennal sockets, clypeus, labrum, genal area, vertex. Antennal sockets in lower half of face. Clypeus protruding, much shorter than broad (0.9-mm width to 0.35-mm length). Punctation on clypeus coarse, denser than on supra-antennal area. Mandible mostly brown, tips darkened, with long dense hair (Fig. 6B). Pre-apical teeth absent, outer ridge strongly developed. Labrum broader than long. Width of compound eye about 1.6× the width of genal area in lateral view (Fig. 6A). Deep, pit-like punctation evenly distributed on supraclypeal area, supra-antennal area, frons, vertex (Figs. 5D and 6B). Protrusions on frontal area absent. Flagellum with 10 flagellomeres. FL1 with 0.14- to 0.16-mm width to 0.11- to 0.12-mm length. FL2 (0.16- to 0.18-mm width to 0.07- to 0.09-mm length) about twice as broad as long and F3 with 0.18- to 0.19-mm width to 0.10- to 0.11-mm length. Last flagellomere about as long as broad: 0.19- to 0.21-mm width to 0.18- to 0.22-mm length. Scape 0.21- to 0.23-mm long. Coloration dark brown. Diameter of lateral ocellus 0.16–0.18 mm, median ocellus 0.18–0.20 mm. Ocellocular distance 0.39–0.41 mm. Mesosoma: As in female but darker (Fig. 6A). Intertegular distance 1.56–1.7 mm. Metasoma: Integument predominantly brown to dark red. Basal areas of terga darker. T1 with split basal patch of thick white setae. T2–T5 with basal bands of setae. T6 with two patches of white setae (Fig. 6D). Punctation on T1–T5 coarse, interspaces smaller than pit diameters (Fig. 6C). T7 with pitted pygidial plate (Fig. 6D). S6 with single median patch of white setae. Remaining visible sterna unmodified.

Etymology

Like in its sister species *S. elizabethae* and in the more robust *S. emmae*, males of *S. gretae* have only 10 flagellomeres. For most known bee species, males have 11 flagellomeres and females have 10. This characteristic is therefore usually associated with females, which is why Bossert (2019) continued with female first names for the genus *Schwarzia*. Herein, we designate female first names for the species that share the character of 10 flagellomeres in males. The species is named after the newborn niece of the first author, Greta Bossert.

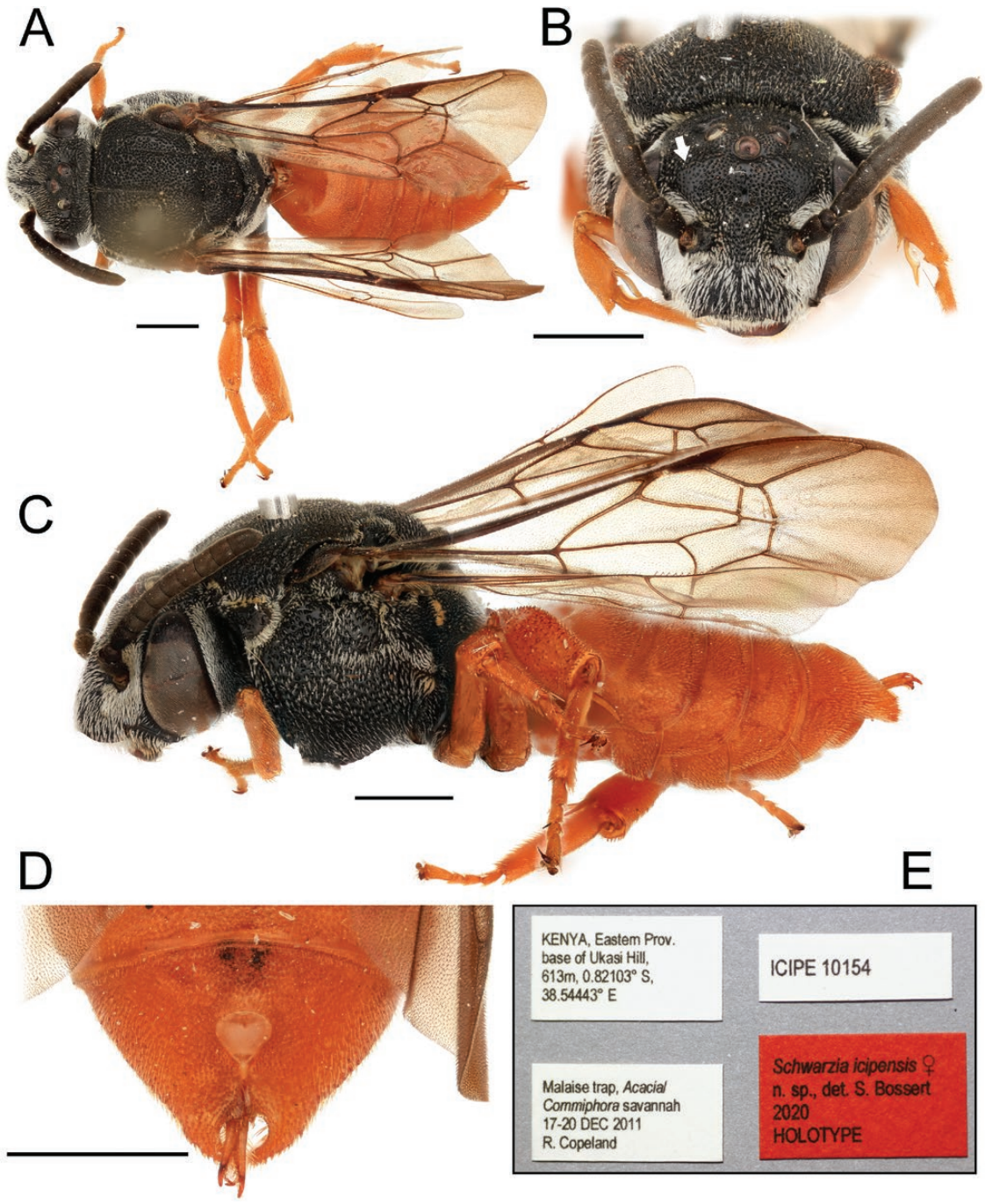

Fig. 7. Female holotype of *Schwarzia icipensis* **sp. nov.** (A) Habitus, dorsal view. (B) Habitus, frontal view. Arrow points to region of supra-antennal area with slightly less dense punctation than surroundings. (C) Habitus, lateral view. (D) Details of T4–T5. (E) Label information as deposited with the holotype. Scale bars show 1 mm.

Distribution

The species is only known from the type locality near Ukasi in Kitui County, Kenya (Figs. 3 and 4A and B).

Remarks

COI sequence data from a paratype specimen can be found under process ID SCHW003–19 in the Barcode of Life Data System.

Schwarzia icipensis Bossert, **sp. nov.**

Figures 7 and 8, 10C, and 11B

Habitat Photograph: Fig. 4A

(urn:lsid:zoobank.org:act:947C8148-2BBB-4C2A-A052-A71E3BD0C132)

Material Examined

HOLOTYPE: KENYA: Eastern Province, base of Ukasi Hill, 0.82103°S, 38.54443°E, 613 m, 17.–20.XII.2011, leg. R. Copeland, Malaise trap, *Acacia*/*Commiphora* savanna, ♀, ICIPE identifier #10154, dep. NMK. Labels of the holotype specimen are shown in Fig. 7E.

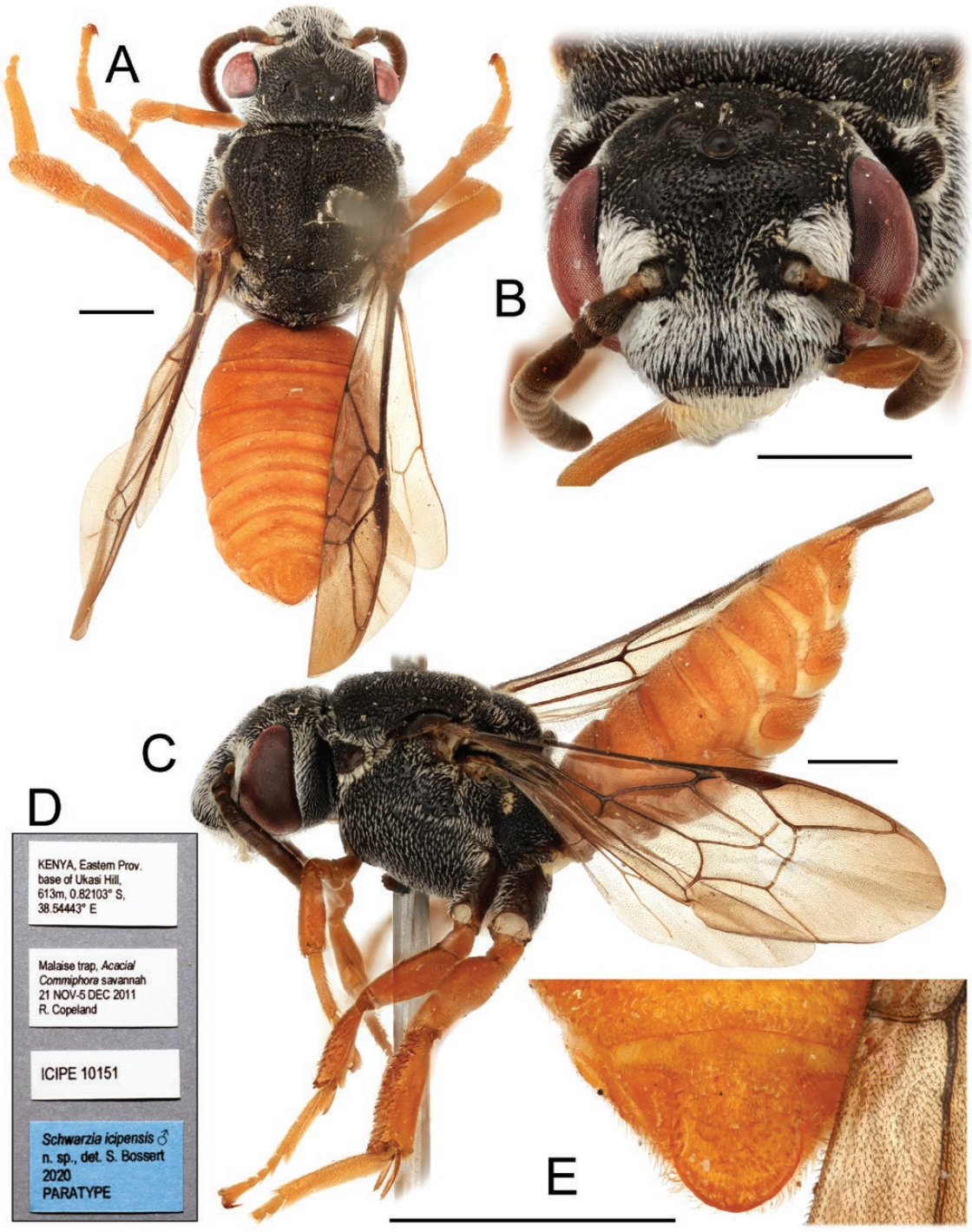

Fig. 8. Male paratype of *Schwarzia icipensis* **sp. nov.** (A) Habitus, dorsal view. (B) Habitus, frontal view. (C) Habitus, lateral view. (D) Label information as deposited with the paratype. (E) Details of T7. Scale bars show 1 mm.

PARATYPES: KENYA: Eastern Province, base of Ukasi Hill, 0.82103° S, 38.54443° E, 613 m, 17.–20.XII.2011, leg. R. Copeland, Malaise trap, *Acacia*/*Commiphora* savanna, 1♀, dep. ICIPE. Eastern Province, base of Ukasi Hill, 0.82103°S, 38.54443°E, 613 m, 1.–6.I.2012, leg. R. Copeland, Malaise trap, *Acacia*/*Commiphora* savanna, 1♀, dep. coll. Bossert. Eastern Province, base of Ukasi Hill, 0.82103°S, 38.54443°E, 613 m, 21.XI–5.XII.2011, leg. R. Copeland, Malaise trap, *Acacia*/*Commiphora* savanna, 1♂, ICIPE identifier #10151, dep. ICIPE.

Diagnosis

Body size 8.2 mm in male, 7.8–8.5 mm in female. *Schwarzia icipensis* differs from all other species of *Schwarzia* by the bright orange-colored integument of the metasoma and the legs, which are in strong contrast to the all-black mesosoma (Figs. 7 and 8). Otherwise, *S. icipensis* is somewhat morphologically similar to *S. emmae* and shares the following characteristics. The punctation on T1 and T2 is fine and not coarse as in *S. elizabethae* and *S. gretae* (Fig. 10C and D). The axillae are flat and not produced as in *S. elizabethae*

and *S. gretae* (Fig. 10A and B). The pygidial plate of males is shield-shaped (Fig. 8E) and not squared as in *S. lualenyiensis*. *Schwarzia icipensis* differs from *S. emmae* as follows. No protrusions are present on the supra-antennal area and the area is more or less evenly punctate (Figs. 7B and 8B). The margin of the compound eye is entire, not indented as in *S. emmae* (Figs. 7C and 8C). The antenna in males has 11 flagellomeres, which is a characteristic only shared with *S. lualenyiensis*. The metanotum is dorsally projecting, much stronger than in *S. emmae*, but not as distinct as in *S. gretae*.

Description

Female (Fig. 7). Head: Head (Fig. 7B) wider than long (2.2- to 2.4-mm width to 1.8- to 1.9-mm length). Integument black except mandible brown. Thick short setae around antennal sockets, on clypeus, and genal area. Clypeus protruding, about twice as broad as long (1.0- to 1.1-mm width to 0.4- to 0.45-mm length). Punctation on clypeus denser and slightly finer than on supra-antennal area. Mandible brown with darkened tip, weakly developed pre-apical tooth and well-developed outer ridge. Setae short and sparse. Labrum broader than long. Proboscis short. Width of compound eye at least 2.5× broader than genal area in lateral view (Fig. 7C). Punctation more or less evenly distributed on supra-antennal area, frons, vertex. Slightly denser on supraclypeal area (Fig. 7B), most coarse on vertex. Interspaces shiny. Granulose protrusions absent but punctation in area where those occur in *S. emmae* slightly weaker. Flagellum with 10 flagellomeres. FL1 as long as broad, 0.20-mm width and 0.19- to 0.20-mm length. FL2 (0.19- to 0.21-mm width to 0.13- to 0.16-mm length) and FL3 (0.22- to 0.24-mm width to 0.15-mm length) broader than long (Fig. 7B). Last flagellomere longer than broad (0.21- to 0.22-mm width to 0.31- to 0.35-mm length). Scape 0.22- to 0.23-mm long. Coloration dark brown. Diameter of lateral ocellus 0.18–0.19 mm, median ocellus 0.20–0.23 mm. Ocellocular distance 0.39–0.42 mm. Mesosoma: Integument entirely black except all leg segments from trochanter to tarsus bright orange (Fig. 7). White setae sparse, primarily along episternal and scrobal groove, around pronotal lobe, metanotum, propodeum. Intertegular distance 1.8–2.0 mm. Axillae not produced nor lamellate (Fig. 11B). Metanotum not or just weakly protruding dorsally (Fig. 11B). Punctation on scutum deep, irregular. Pit diameter slightly larger than on vertex. Scutum without elevated parallel ridges adjacent to mesoscutellar line. Omaulus lamellate. Punctation on scutellum as on scutum. Wing venation brown. Meso- and metatibial spurs with two ventrally oriented rows of teeth. Metasoma: Integument entirely bright orange, without tergal bands. Punctation on T1–T5 similarly fine and dense, interspaces smaller than pit diameters (Fig. 10C). Disc of T5 with pseudopygidial plate which is about as broad as long (Fig. 7D). Posterior T5 with two hook-shaped projections medio-laterally, which form genus-specific opening through which bifid S6 protrudes. Hook-shaped projections robust, forming a narrow opening, which is about as broad as pseudopygidial plate. Punctation on basal areas of S2–S5 fine and tesselate. Punctation on discs denser and deeper, interspaces shiny. Integument of basal, median, and posterior areas of sterna of similar coloration. S1–S5 without distinct patches of setae.

Male (Fig. 8). Similar to female except terminal terga. Head: Head (Fig. 8B) wider than long (width 2.2 mm, length 1.8 mm). Thick short setae primarily around antennal sockets, on paraocular, clypeus, and genal area. Clypeus protruding, more than twice as broad as long (1.2-mm width to 0.4-mm length). Punctation more or less evenly distributed on supra-antennal area, clypeus, frons. Densest on supraclyeal area and most rugose on vertex. Mandible dark with very weakly developed pre-apical tooth and well-developed outer ridge. Mandible with long dense hair (Fig. 8B). Labrum broader than long. Proboscis short. Width of compound eye about 1.8× the width of genal area in lateral view (Fig. 8C). Distinct granulose protrusions on frontal area absent; instead with slightly finer punctation. Flagellum with 11 flagellomeres. FL1 about as broad as long (0.18-mm width to 0.17-mm length). Both FL2 (0.21 mm width to 0.12 mm length) and FL3 (0.22 mm width to 0.14 mm length) much wider than long. Last flagellomere longer than broad: 0.20-mm width to 0.24-mm length. Scape 0.3 mm long, integument dark. Diameter of lateral ocellus 0.18 mm, median ocellus 0.20 mm. Ocellocular distance 0.43 mm. Mesosoma: As in female (Fig. 8A). Intertegular distance 1.9 mm. Metasoma: As in female except of terminal terga. Punctation on T6 more rugose than on preceding terga. T7 with pitted pygidial plate (Fig. 8E). All visible terga and sterna without distinct patches of setae. Punctation on sternal discs denser and deeper than on basal areas, interspaces shiny. Basal areas of S2–S5 with lighter-colored integument than median and posterior areas.

Etymology

The species is named in honor of the International Centre of Insect Physiology and Ecology (ICIPE) in Nairobi Kenya. ICIPE facilitates research in all areas of entomology in Eastern Africa and was instrumental in the preparation of this study.

Distribution

Like *S. gretae*, this new species is only known from the type locality near Ukasi in Kitui County, Kenya (Fig. 4A and B).

Remarks

The striking color pattern with an all-black mesosoma and bright orange metasoma in *S. icipensis* is different from any other species of *Schwarzia*, but represents a common color pattern of bees in the Afrotropical region. Several lineages of cleptoparasitic Apidae (e.g., *Ammobates* Latreille, 1809, *Pasites* Jurine, 1807, *Sphecodopsis* Bischoff, 1923), cleptoparasites of other families (*Euaspis* Gerstäcker, 1857 (Megachilidae), *Eupetersia* Blüthgen, 1928, *Sphecodes* Latreille, 1804 (both Halictidae)), and other non-parasitic bees (*Spatunomia* Pauly, 1980 (Halictidae), *Mermiglossa* Friese, 1912 (Andrenidae)) possess this or very similar color patterns. Because these bees are not closely related, this indicates a widespread ring of Müllerian mimicry. Otherwise, the gestalt of *S. icipensis* resembles that of *S. emmae* on first sight. However, there are significant morphological differences between the species as described above, and they are not sister taxa (Fig. 1). *Schwarzia emmae* is part of the clade that has the antenna in males reduced to 10 flagellomeres whereas *S. icipensis* is not. COI sequence data from a paratype specimen can be found under process ID SCHW005–19 in the Barcode of Life Data System.

Schwarzia lualenyiensis Bossert, **sp. nov.**

Fig. 9

(urn:lsid:zoobank.org:act:CBA82B37-EBBA-470E-AAE9-CFEB692E8683)

Material Examined

HOLOTYPE: KENYA: Taita-Taveta County, Lualenyi, 3.5458°S, 38.3112°E, 1,010 m, 10.VI.2013, in pan trap, leg. P. Steward, ♂, ICIPE identifier #10155, dep. NMK. Labels of the single type specimen are shown in Fig. 9E.

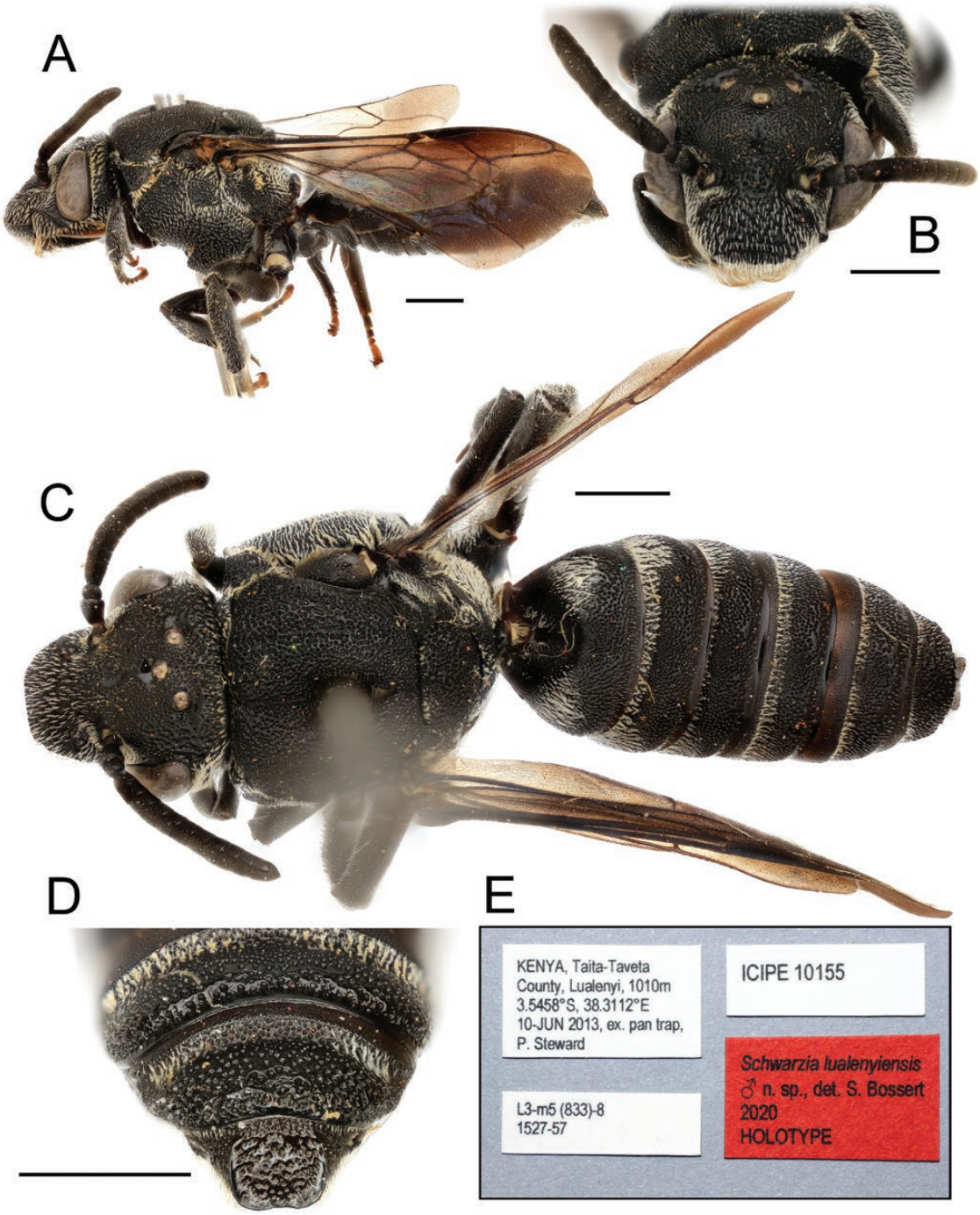

Fig. 9. Male holotype of *Schwarzia lualenyiensis* **sp. nov.** (A) Habitus, lateral view. (B) Habitus, frontal view. (C) Habitus, dorsal view. (D) Details of T7. (E) Label information as deposited with the holotype. Scale bars show 1 mm.

Diagnosis

Body size 10.4 mm in male. *Schwarzia lualenyiensis* is a very distinct species and differs from all other species of *Schwarzia* in several characters. It is larger than all other known species. It has a conspicuously strongly produced clypeus (Fig. 9C), that is much more protuberant than in the other species (cf., Fig. 10A and B). The forewing is strongly darkened over its entire length and is much darker than the hindwing (Fig. 9A), as well as the wings of the other species. It is the only species in which the integument of the tegula is nearly entirely black. It is further the only species in which the male pygidial plate on T7 is square shaped and not shield shaped (Fig. 9D). The marginal zones of T1–T4 have a clearly visible line without any punctation apically, whereas the punctation in all other species reaches very close to the border of the respective segments. The punctation on T1 and T2 is intermediate to those of the other groups: it is finer than in *S. gretae* and *S. elizabethae*, but coarser than in *S. emmae* and *S. icipensis*. The integument of *S. lualenyiensis* is entirely black and hence different than in *S. elizabethae* and *S. gretae*. The axillae are flat and not produced as in *S. elizabethae* and *S. gretae*. *Schwarzia lualenyiensis* further differs from *S. emmae*

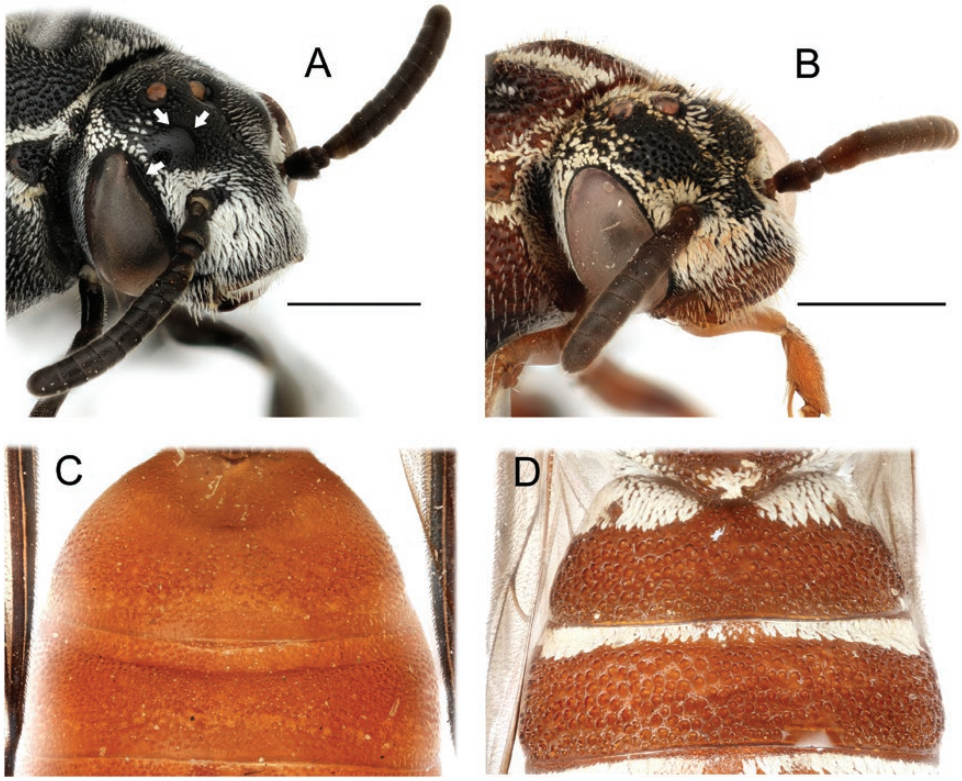

Fig. 10. Characteristic morphological features of different species of *Schwarzia*. (A) Head of female *S. emmae,* anterior dorsolateral view. The upper two arrows point to granulose protrusions on the supra-antennal area, the lower arrow points to the indented inner margin of the compound eye. (B) Female paratype of *S. gretae* in same view. The supra-antennal area is evenly punctate and the inner margin of the compound eye is not indented. (C) Details of T1–T2 of *S. icipensis* (♀, paratype). (D) Details of T1–T2 of *S. gretae* (♀, paratype). Scale bars show 1 mm.

by the lack of granulose protrusions on the frontal area, but the margin of the compound eye is indented. Like in *S. icipensis*, the male antenna has 11 flagellomeres.

Description

Male (Fig. 9). Head: Head wider than long (2.5-mm width to 2.2-mm length). Integument entirely black with white setae on clypeus, labrum, genal, and paraocular area. Antennal sockets in lower half of frons. Clypeus strongly protuberant (Fig. 9A and C), more than twice as broad as long in frontal view (1.4-mm width to 0.6-mm length). Punctation on clypeus and supra-clypeal area coarse, deep, irregular. Interspaces shiny. Punctation finer and denser on frons and supra-antennal area (Fig. 9B). Punctation more rugose and coarser on vertex, with shiny pit-free areas adjacent to outer ocellus (Fig. 9C). Mandible dark, thin, with long tuft of yellowish hair (Fig. 9B). Preapical tooth absent or just very minutely produced, outer ridge strongly developed. Labrum slightly broader than long. Proboscis not particularly long, about as long as the head in lateral view. One maxillary palpomere visible in holotype, presumably the only palpomere of the maxillary palps. Width of compound eye exceeds the width of genal area but is relatively shorter than in other species of *Schwarzia*, about 1.3× as broad as genal area (Fig. 9A). Flagellum with 11 flagellomeres. FL1 about as long as broad (0.2-mm length to 0.19-mm width), FL2 clearly longer than broad (0.26-mm length to 0.13-mm width) and FL3 as long as broad (0.16-mm length to 0.15-mm width). Coloration entirely black. Diameter of outer ocellus 0.21 mm, median ocellus 0.22 mm. Ocular ocellar line 0.53 mm. Mesosoma: Entire integument black, including legs and pronotal lobe (Fig. 9A). Only terminal tarsomeres with lighter coloration, browned. Setae creamy-white, rather sparse, primarily present on borders between segments as described for the other species. Densest coverage of setae on propodeal surface, except of propodeal triangle. Intertegular distance 2.3 mm. Axillae weakly produced. Punctation on scutum slightly coarser and more irregular than on frons. Interspaces shiny but small and irregular, not more than the pit diameter. Punctation on scutellum coarser than on scutum and irregular, punctation finer toward the anterior border. Integument of tegula nearly entirely black (Fig. 9C). Wing venation black. Forewing strongly darkened over its entire length, hindwing largely clear. Hind leg with 2 tibial spurs, mid leg with single spur. Tibial spurs similarly enlarged and with ventrally oriented rows of teeth as in the other species. Metasoma: Integument entirely black, including marginal zones of all visible terga. Marginal zones of T1–T4 with distinct shiny line without any punctation. Vertical area of T1 deeply emarginated. T1 with two lateral patches of thick white setae. T2–T4 with basal bands of white setae, which may be covered by the apical margin of neighboring tergum. Basal band of setae on T5 indistinct. Punctation on T1–T3 distinctly finer than on T4–T6, where punctation becomes increasingly coarse and irregular. Interspaces shiny. T7 with distinctly pitted pygidial plate, which is square shaped (Fig. 9D). S5–S6 covered with white setae.

Etymology

The species is named after the Lualenyi area of Taita-Taveta County, located in southeastern Kenya.

Distribution

The species is only known from the type locality.

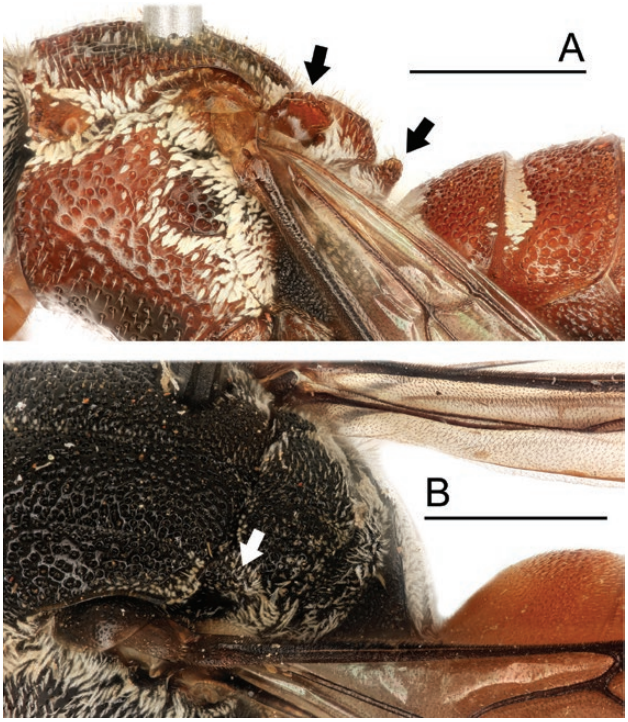

Fig. 11. Morphological differences between species of *Schwarzia*. (A) Mesosoma of *S. gretae* in lateral view (♀, paratype). Left arrow points to the produced, lamellate axilla. Right arrow points to the produced, dorsally protruding metanotum. (B) Posterior dorsolateral view of *S. icipensis* (♀, paratype). The axillae are not produced or lamellate. Scale bars show 1 mm.

Remarks

The species is only known from the single male holotype. The specimen was collected in a pan trap, placed about 5 m in the bush from the edge of a field (Peter Steward, pers. communication). COI sequence data from the holotype can be found under process ID SCHW004–19 in the Barcode of Life Data System.

Identification Key to the Species of *Schwarzia* Eardley, 2009

1 Clypeus strongly protruding (Fig. 9A–C); forewing very dark; entire integument black; compound eye not broader than 1.3× the width of the genal area in lateral view. ♂: pygidial plate square-shaped (Fig. 9D). ♀: unknown. Largest known species of the genus (> 10 mm) ..... *Schwarzia lualenyiensis* Bossert, **sp. nov.**

1’ Clypeus not particularly developed (e.g., Figs. 5C, 7C, 8C, and 10A and B); forewing clear or just slightly darkened anteriorly; integument black or red to orange and black; compound eye at least 1.6× the width of the genal area in lateral view ♂: border of pygidial plate rounded posteriorly, shield-shaped (Figs. 6D and 8E). Smaller species (<9 mm) 2

2 Supra-antennal area with distinct, finely pitted protrusion (Fig. 10A); inner margin of compound eye indented ..... *Schwarzia emmae* Eardley, 2009

2’ Supra-antennal area without protrusion (Fig. 10B), at most with a few fine pits that are not clearly set off the surrounding area (Fig. 7B, indicated by white arrow); inner margin of compound eye not indented 3

3 Axillae lamellate and produced (best seen in lateral view; Fig. 11A); punctation on T1–T2 coarse (Fig. 10D); at least T1–T4 with basal patches or bands of white setae (Figs. 5A and C and 6C); integument of metasoma black and/or red to reddish orange, but if red to reddish orange, then at least with patches of reddish integument on mesosoma (Figs. 5A and 5C and 6C). ♂: antenna with 10 flagellomeres 4

3’ Axillae not lamellate or produced (Fig. 11B); punctation on T1–T2 fine (Fig. 10C); terga without patches or bands of white setae; entire metasoma and all legs bright orange while integument of mesosoma all black (Fig. 7A and C). ♂: antenna with 11 flagellomeres ..... *Schwarzia icipensis* Bossert, **sp. nov.**

4 Metasoma (and to a lesser extent mesosoma) with significant parts of orange or reddish orange integument (Figs. 5A and C and 6C); axillae strongly produced and lamellate, tip usually reddish-orange; metanotum strongly produced, protruding dorsally (Fig. 11A); scutum with ridges along mesoscutellar line (best seen in frontal view; Figs. 5B and 6B, indicated by arrows). ♀: posterior opening of T5 wider and more rounded (Fig. 5E) than in alternate. Slightly larger (6.1–7.5 mm) ..... *Schwarzia gretae* Bossert, **sp. nov.**

4’ Integument of meso- and metasoma entirely black, usually only junctions between segments with lighter browned integument, i.e., junction between terga, on callus, coxa, etc. (Bossert 2019, their Figs. 1A and 3A); axillae more weakly produced than in alternate, tip black; metanotum produced but just weakly protruding (Bossert 2019, their Figs. 1C and 3C); ridges along mesoscutellar line weakly developed. ♀: posterior opening of T5 narrower, more elliptically shaped (Bossert 2019, their Fig. 3E). Slightly smaller (5.1–5.9 mm) ..... *Schwarzia elizabethae* Bossert, 2019

Townsendiella Crawford, 1916

Type species: *Townsendiella pulchra* Crawford, 1916

= *Xeropasites* Linsley, 1942. Type species *Townsendiella rufiventris* Linsley, 1942

= *Eremopasites* Linsley, 1942. Type species *Townsendiella californica* Michener, 1936

Diagnostic Characters

Adults: The genus *Townsendiella* can only be diagnosed by a unique combination of characters that are not unique among Neolarrini. The shape of the apex of the marginal cell of the forewing is slightly pointed and terminates separate from the wing margin. The profile of the propodeum is convex and vertical in *T. pulchra* and without a distinct horizontal basal area. However, it is rather convex (as in most Neolarrini) in other species of *Townsendiella*. *Townsendiella* has simple mandibles, without a preapical tooth, and a medially pointed labrum as in *Rhopalolemma* and *Neolarra*. The second tarsomere of the foretarsus is distinctly asymmetrical as in *Rhopalolemma*, yet weaker developed. The pygidial plate of T6 in females and T7 in males is well developed. Scale-like setae are present on the entire body, frequently also on the propodeal triangle (metapostnotum), similar to *Neolarra*. The forewing has two submarginal cells and the length of the second submarginal cell is somewhat reduced; it is nearly two times shorter than the first. The first recurrent vein joins the first or the second submarginal cell, but it is always very close to the first submarginal crossvein or even interstitial. The pseudopygidial area of tergum 5 of females is absent in three species, but present in *T. rufiventris* Linsley, 1942 (Orr and Griswold 2015).

Larvae: The mature larva of *Townsendiella* is distinct from those of other Neolarrini by having a particularly wide head capsule, with parietals so strongly developed that the head capsule appears to have

a median depression in frontal view (Rozen and McGinley 1991, their Fig. 8).

Egg chorion: The egg chorion of *Townsendiella* is simple; lamellate tubercles are not developed.

Species included:
Townsendiella californica Michener, 1936
Townsendiella ensifera Orr and Griswold, 2015
Townsendiella pulchra Crawford, 1916
Townsendiella rufiventris Linsley, 1942

Discussion

Revisionary Taxonomy

We outlined three central problems that so far prevented a thorough reevaluation of biastine taxonomy: 1) The hypothesized but untested paraphyly of *Biastes* with respect to *Neopasites*, 2) the lack of molecular data to settle the disparate phylogenetic signal on the phylogenetic placement of *Rhopalolemma*, and 3) the unknown phylogenetic relationship of *Schwarzia* to other parasitic Apidae. The results presented in this study, which integrate insights from phylogenomics and morphology of adult and immature life stages, allow us to address these problems and develop a comprehensive reevaluation of the taxonomy of *Biastes* and related lineages.

Neopasites is a Subgenus of *Biastes*

Biastes and *Neopasites* as used previously (e.g., by Michener 2007, Ascher and Pickering 2020; Fig. 2) each comprise five described species from the Nearctic (*Neopasites*) and Palearctic (*Biastes*). Clear diagnostic features to separate the groups using morphology proved difficult to obtain. Michener's (2007) identification key uses size ratios of the two submarginal cells but this character fails to identify *B. truncatus* (and other *Melittoxena*) as *Biastes* (Fig. 2). In these species, the second submarginal cell is shorter than the first, as in *Neopasites*. The most decisive character used in Michener's (2007) key is the shape, position and pubescence of the pseudopygidial area on the fifth tergum of females. This character, which is illustrated in Bossert (2019, their Fig. 7), allows the separation of females but is not sufficient to justify the recognition of separate genera under the requirement of natural groups (Figs. 1 and 2). Roig-Alsina (1991) indicated a possible paraphyly of *Biastes* in respect to *Neopasites* because of the pointed sting shape of *Biastes truncatus*. His study found the sting of other examined *Biastes* and *Neopasites* to be bifid apically, thus indicating a paraphyletic *Biastes* (Roig-Alsina 1991). It is this exact species (*B. truncatus*) that renders *Biastes* in the old sense paraphyletic in our study (Figs. 1 and 2). Interestingly, the same species was regarded as distinctly different and was transferred into a new genus *Melittoxena* in one of the earliest treatments of the group, nearly 150 yr ago (based on the above mentioned differences in wing venation; Morawitz 1873). *Melittoxena* was synonymized with *Biastes* shortly thereafter (Radoszkowski 1874, Friese 1895) and gained little subsequent attention in the field. However, it was resurrected by Popov (1933), who uses *Melittoxena* as a subgenus of *Biastes* based on comparative studies of male genitalia and terminal sterna. Despite careful illustrations, this work was not adopted by a broad scientific community either, likely because of language barriers and limited dissemination (but see Proshchalykin and Lelej 2004).

Our integrative assessment of the relationships of *Biastes* reveals the recognition of *Melittoxena* as our preferred approach to solving the problem of the paraphyly of *Biastes*. *Melittoxena* has clear morphological features and is diagnosable in both sexes. Its close relationship to the North American taxa is supported by molecular data, as well as morphological and biological similarities. As far as we know, all North American *Biastes* (subg. *Neopasites*) are brood parasites of *Dufourea*, and so is *B.* (*Melittoxena*) *truncatus*, whereas the Old World *Biastes* s. str. use hosts of different genera (Fig. 2; '*Dufourea* clade'). *Biastes* (*Melittoxena*) *popovi*, for which hosts have not yet been observed, occurs in areas in which the only rophitine bees are *Dufourea* as well (Proshchalykin and Lelej 2004).

Lastly, we formally synonymize the North American subgenera *Neopasites* s. str. and *Micropasites*, which were recognized by Michener (2007) for *Neopasites* (Fig. 2). These two groups are both species-poor and very similar in their morphology. The main differences are the slightly larger body size of *Neopasites* and the distinctly reduced maxillary palps of *Micropasites*. Even though these differences are unambiguous, they do not suffice to support monophyly of the two species placed in the nominotypic subgenus *Neopasites*, as this group does not have any distinct apomorphic characters at the subgeneric level. The single distinguishing character of *Micropasites* is potentially a reduction of an ancestral state and could be connected to the overall reduction in body size.

Rhopalolemma is the Sister Genus to *Townsendiella*

Members of the genus *Rhopalolemma* are rarely collected, enigmatic bees with previously unclear phylogenetic relationships. Conflicting phylogenetic signals of immature and adult morphological features render them a seemingly transitional form between *Biastes* and *Townsendiella*. Roig-Alsina (1991) described *Rhopalolemma* based on a single female adult and noted a resemblance with *Townsendiella*, but he also found internal structures, particularly those of the sting apparatus, to be synapomorphic with *Neopasites*. Based on a cladistic analysis of 22 adult morphological characters, he concluded that *Rhopalolemma* is 'quite divergent, yet obviously a member of [this tribe]' Biastini, i.e., of *Biastes* and *Neopasites* as used previously (Fig. 2). A subsequent study significantly improved our understanding of the biology of *Rhopalolemma* through field observations, the description of a new species from both sexes, and detailed accounts of immature stages (Rozen et al. 1997). Their cladistic analyses, however, revealed conflicting information regarding the phylogenetic position of the genus. While larval morphological characters support a sister group relationship to *Townsendiella*, adult and oocyte morphology indicate a closer relationship to *Neopasites*.

The molecular evidence presented herein allows us to shed light on this issue. Phylogenomics strongly supports a sister group relationship of *Rhopalolemma* and *Townsendiella* and indicates that larval similarities of these two groups are likely true synapomorphies (Fig. 2). Adult morphological characters that supported *Rhopalolemma* + *Biastes* previously, such as the absence of a membranous flap on the S6 of female, the presence of a lateral keel on the same structure, and the absence of stipital combs (Roig-Alsina 1991, Rozen et al. 1997) appear plesiomorphic under this topology. However, certain presence/absence characters, such as the loss or reduction of the stipitial comb, have evolved in multiple bee groups and are likely associated with a parasitic lifestyle (Michener 2007). The *Rhopalolemma* lineage diverged from the MRCA of *Biastes* around 43.0 mya and slightly later (39.6 mya) from *Townsendiella*. This long period provided ample time to acquire morphological and potential convergent change, especially since all these bees use closely related hosts, co-occur in the same habitats, and feed on the same few seasonally abundant floral resources (Rozen et al. 1997). This applies to *Townsendiella* and *Neolarra* as well, which are the only bees of Neolarrini in the new

sense which do not all attack Rophitinae (Fig. 2). Losses and/or reductions of structures could represent adaptive features associated with changing life history traits over the past 46 million years in Neolarrini.

Lastly, the placement of *Townsendiella* requires a taxonomic change, since it renders Neolarrini in the new sense (and also the former Biastini) paraphyletic (Fig. 2). We compared the two possible options to solve this problem: 1) Raise *Rhopalolemma* to its own tribe Rhopalolemmini, representing only two described species and diagnosable by few morphological characters that are largely of internal nature and hard to access. This would have allowed retention of Townsendiellini, another monogeneric tribe with only five species, as well as Biastini with *Biastes* + *Schwarzia* (now 15 described species). Alternatively, 2) unite all three lineages in a larger tribal concept that provides better diagnosability and avoids oversplitting at tribal level. The cleptoparasitic Apidae seem already overly subdivided, as they represent only about 7.9% of all described bee species but nevertheless comprise 27.2% of all bee tribes, several of which are monogeneric (numbers based on data from the Discover Life database, Ascher and Pickering (2020)). We therefore decided to sink the tribe Townsendiellini into a larger tribal framework. Evaluating alternative two further revealed a much greater suite of morphological diagnostic characters for adults, mature, and first-instar larvae, as well as eggs, when including the sister group to the former Biastini, *Neolarra* (see characters in Fig. 2). Since *Neolarra* is also the sole representative of its tribe Neolarrini, we argue that consolidation of these lineages into a comprehensive tribal framework better represents their phylogenetic relationships and will facilitate future research on this group.

The tribe Neolarrini in this new sense can be diagnosed by multiple characters that can be expected to be apomorphic or plesiomorphic (Fig. 2). However, polarization of these characters cannot be sufficiently assessed without a comprehensive analysis with phylogenomic data of a much wider sampling of nomadine taxa. Several diagnostic characters are likely shared with bees of the tribe Hexepeolini, to which the tribe Neolarrini may be most closely related (Policarová et al. 2019). In contrast, other characters seem to be shared with phylogenetically much more distantly related cleptoparasitic tribes, such as Caenoprosopidini, which also have robust pedicels and only two submarginal cells. These characters therefore almost certainly evolved convergently and may be related to parasitism or miniaturization. In the particular case of distinguishing Neolarrini from Hexepeolini, these characters have practical importance despite their likely plesiomorphic nature.

Schwarzia

In the initial description of *Schwarzia*, Eardley (2009) recognized it as Biastini and proposed a particularly close relationship to *Biastes*. This was a remarkably accurate assessment based on morphological examination, which we herein confirm with molecular data. In fact, *Schwarzia* is sister group to *Biastes* as proposed above (Figs. 1 and 2). In a second account of *Schwarzia*, Bossert (2019) described a second species and reevaluated the morphology of the genus. Some characters that were previously thought to be diagnostic for Biastini (except *Rhopalolemma*), such as the bidentate mandibles, did not hold up for the second species. However, other newly discovered features, including the reduced number of flagellomeres in males and the broad shape of the labrum, supported its morphological affinity to *Biastes*.

The description of three new species of *Schwarzia* herein demolishes one of these re-defined features. Both *Schwarzia icipensis* and *S. lualenyiensis* possess 11 flagellomeres in the male. Interestingly, there is also a single species of *Biastes* with 11 flagellomeres (*B. brevicornis*), whereas males of other *Biastes* possess 10. In *Schwarzia*, this trait is phylogenetically conserved, as species with 11 flagellomeres in males are sister taxa. The other three *Schwarzia* species, all of which have only 10 flagellomeres in the male, form the sister clade to this grouping (Figs. 1 and 2). Based on this, we decided to continue assigning female first names only to those new species of *Schwarzia* that exhibit this trait. We further reevaluated the shape of the labrum of *Schwarzia* and discovered a shared morphological feature with *Biastes*. In both *Biastes* and *Schwarzia*, the apical margin of the labrum is straight, whereas it is medially prolonged and apically rounded or nearly pointed in all other Neolarrini. Besides these features, we report seven diagnostic characters for the genus *Schwarzia*, nearly half of which stem from the terminal segments of the female metasoma (Fig. 2).

Historical Biogeography

To date, the historical biogeography of Neolarrini or the former Biastini has only been studied superficially. This can primarily be explained by the lack of phylogenetic knowledge of the exact relationships among the many different tribes of cleptoparasitic Apidae. It has only recently been established that most of the cleptoparasitic Apidae, a morphologically diverse and heterogeneous group, form an approximately 100 mya old natural group (Cardinal et al. 2010, Litman et al. 2013). Without this knowledge, Michener (1979) briefly discussed the tribal biogeography of Biastini in its former sense, i.e., with the North American *Neopasites* and the Palearctic *Biastes*. Taking the primarily Western Nearctic distribution of *Neopasites* s. l. into account, he speculated on a dispersal over the Bering Strait, but was not able to discuss direction, antiquity or geographical origin of the group. The present study, which is the first attempt to explain the phylogeography of *Biastes* with a fossil-calibrated molecular data set, allows us to shed light on these long-standing questions.

Our results strongly support a Palearctic origin of *Biastes*, whereas the tribe Neolarrini in the new sense most likely originated in North America. The two earliest branching lineages of Neolarrini, *Neolarra* and *Townsendiella* + *Rhopalolemma*, are both exclusively Nearctic, strongly indicating a presence of the MRCA of Neolarrini in North America. Using the best-fitting DIVA-like model, it seems most likely that the MRCA of *Biastes* and *Schwarzia* traversed from the New World to the Palearctic in the mid Eocene (Fig. 1). The route of dispersal cannot be confidently determined from today's perspective, but very likely happened over either the Bering Strait or the North Atlantic Land Bridge. At this time, parts of the present-day Bering and Chukchi seas were situated above sea level for consecutive periods, forming a passable land bridge between the Nearctic and Palearctic. A dispersal over the North Atlantic is not unlikely either, as it would have only required the crossing of relatively narrow stretches of water. Despite this uncertainty, our results clearly show that one descendant lineage of this MRCA dispersed to the Afrotropical realm from the Palearctic shortly thereafter and that the descending *Schwarzia* represent a lineage that has been present in the Afrotropical realm for at least ~39 million years.

The Palearctic origin of *Biastes* indicates that the MRCA of the present-day *Neopasites* traversed from the Palearctic to the Nearctic. Our divergence time estimates indicate that this happened in the mid Miocene (~15.4 mya). During this time period, the Bering Strait formed a relatively broad land bridge between the Eastern Palearctic and the Western Nearctic, whereas the North Atlantic route would have required crossing significant stretches of water (Fig. 12). While

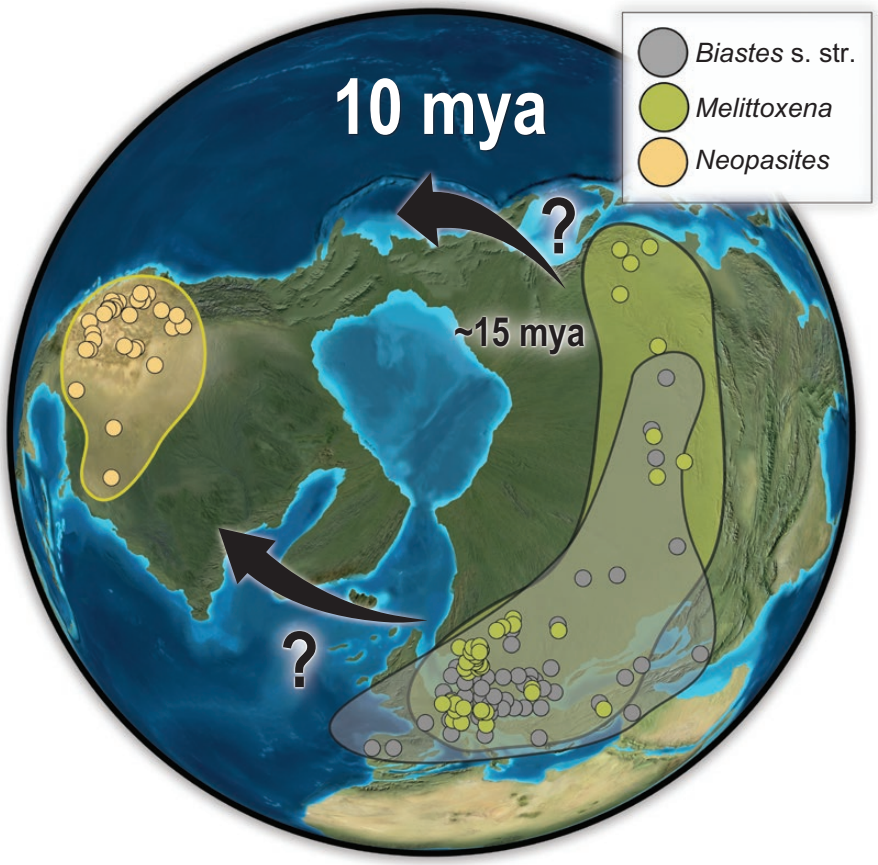

Fig. 12. Present-day distributional records of *Biastes* projected on a global map with reconstructed continental boundaries of the mid Miocene. Shown is a polar projection centered on the Geographic North Pole. During this time peri od, large parts of the present-day Bering and Chukchi seas were likely above sea level, forming a continuous land bridge between the Nearctic and the Palearctic. Locality records are taken from the Discover Life database (Ascher and Pickering 2020) and own databasing efforts. Selected entries were further taken from GBIF (2019). Note that certain Far Eastern records are regional centroids and do not represent exact collection localities.

dispersals over the North Atlantic Land Bridge are well documented for certain groups (e.g., Davis et al. 2002 for Malpighiaceae), this route seems increasingly unlikely after the land bridge broke up by the Eocene (Tiffney 1985, Milne 2006). This, together with today's primarily western distribution of *Biastes* (*Neopasites*) in the Nearctic and the presence of *Biastes* (s. str. + *Melittoxena*) in the northern Far East, renders the dispersal over the Bering Strait the most likely scenario (Fig. 12).

Our assessment of the historical biogeography of Neolarrini is based on the model testing procedure of BioGeoBEARS (Matzke 2018), which allows testing the fit of different biogeographic models in a likelihood framework. This testing procedure includes the +*j* parameter, which takes the probability of jump-dispersals or founder events into account. Usage of this parameter has recently been criticized (Ree and Sanmartín 2018), which is why we also estimated ranges using the best-fitting model excluding +*j*, which was the DEC model (Ree and Smith 2008). The results from this analysis (i.e., without +*j*; Supp Fig. 4 [online only]), however, are more difficult to interpret from the perspective of actual biogeographical events and indicate seven range-changing events in the lineage leading to present-day *Biastes*. The model favors a Nearctic + Palearctic MRCA of Neolarrini with frequent exchanges between these regions during the Miocene and the Eocene. Importantly, however, the MRCA of *Biastes* + *Schwarzia* was most likely also exclusively Palearctic at some point, and *Schwarzia* descendent from a Palearctic ancestor. As results under both models are not strongly conflicting, yet the model using the +*j* parameter provided a more parsimonious scenario that seems more biologically realistic, we favor the results obtained with +*j*.

Host Usage of Neolarrini in the New Sense

Synthesizing the data on neolarrine hosts from the literature and our time-calibrated phylogeny reveals three general patterns. First, with a single potential exception (see below), virtually all known hosts of Neolarrini are oligolectic pollen collectors. Second, most known hosts of Neolarrini excluding *Neolarra* are Rophitinae, and all *Biastes* rely on rophitine hosts. Third, host lineages are older than their parasitic counterparts (Fig. 1), except for two specific cases which are discussed below.

Neolarrini are parasites of specialist pollen collectors: as far as known, all hosts are oligoleges on different host plants (Fig. 2 and literature cited in caption) and some species (e.g., *Systropha* spp.) could even be considered locally monolectic. It is unlikely that this pattern, which holds throughout their entire range, is due to chance. A single exception may be the polylectic *Perdita sexmaculata* Cockerell, 1895, which was considered the host of *Neolarra vigilans* (Shanks 1978). However, it is unclear how this information was obtained and this host–parasite relationship has not been confirmed subsequently. Another unusual association which was proposed in the same paper, *Calliopsis larreae* (Timberlake, 1952) being host to *Neolarra hurdi*, was later dismissed (Rozen 2000).

The general pattern of attacking specialized hosts has implications for the evolution of host–parasite relationships and raises the question to what extent the parasites are 'pollen specialists' themselves. Naturally, their larvae feed exclusively on the pollen provisions of their hosts, but it may not matter entirely for the parasite what specific host species provisions the nest, as long as it collects a specific kind of pollen. Recent studies on oil-collecting bees (Martins et al. 2018, Policarová et al. 2019) revealed a clade of cleptoparasites that are almost exclusively attacking bees that collect and usually provision their brood cells with particular floral oils, and further showed that evolutionary transitions to these specialized hosts are much less likely than to normal pollen collectors. However, once the parasites were able to cope with the specialized provisions, the entire lineage diversified with the specialized hosts for millions of years.

Coincident with the pattern of attacking specialist pollen collectors is the trend that Neolarrini excluding *Neolarra* attack primarily Rophitinae. As nearly all Rophitinae are specialist pollen collectors, it is difficult to differentiate if the parasites are constrained to attack oligolectic pollen collectors, rophitine bees, or both. Host preferences of most Nomadinae appear to be phylogenetically conserved (e.g., *Epeolus* Latreille, 1802 seems to be restricted to *Colletes*, Latreille, 1802, *Melecta* Latreille, 1802 usually parasitizes *Anthophora* Latreille, 1803, etc.) and can be explained by adaptations in the parasitic lineages to efficiently find suitable host nests. Brood cell linings produced by the Dufour's gland of ground-nesting bees are known to serve as semiochemical cues in nest recognition and are often species-specific, yet universal compounds are shared among related lineages (Mitra 2013 and references therein). Cleptoparasitic bees likely use these odor cues to locate their hosts' nests and neolarrine bees may be pre-adapted to locate nests of Rophitinae. Strikingly, Cane (1983) found the Dufour's gland secretions of *Dufourea* (Rophitinae), *Perdita*, and certain Melittidae (including *Hesperapis*) to be highly similar to each other and showed certain aliphatic esters to be characteristic for only these taxa. These groups are distantly related, yet cover the entire host spectrum of Neolarrini in the new sense, making it highly likely that shared chemical compounds in the Dufour's gland secretions of the host bees play a crucial and overlooked role in the host–parasite dynamics for Neolarrini.

However, our data also show that several parasitic bees are not species-specific, but specific only on those bees that collect certain pollen. For every case in which a parasite is known to have more than one host, all host species feed on the same floral resources (Fig. 2). Because their emergence is synchronized with their host plant(s), these host bees naturally co-occur and are active in the same phenological window. This provides an obvious opportunity for a parasite to use several suitable host species. However, switching to a host that uses a different host plant represents a much greater challenge: despite co-occurring locally and phenologically, all three European species of *Biastes* only parasitize those closely related hosts that share the same host plant (Fig. 2). *Biastes truncatus*, for example, attacks both species of *Dufourea* that are *Campanula* specialists (*D. dentiventris* (Nylander 1848), *D. inermis* (Nylander 1848)) but does not parasitize other co-occurring species of *Dufourea* such as *D. minuta* Lepeletier, 1841 or *D. halictula* (Nylander, 1852).

The close host–parasite association of Neolarrini with Rophitinae is particularly clear for *Biastes* as re-defined here, which exclusively attack rophitine bees. Furthermore, there is a clade of *Biastes* comprising the subgenera *Neopasites* and *Melittoxena* that seems to exclusively parasitize *Dufourea*, despite its distribution on different continents (Fig. 2, '*Dufourea*' clade). The affinity toward Rophitinae is less clear in the other groups. The single species of *Rhopalolemma* for which the host has been established follows the pattern (*Protodufourea* Timberlake, 1955 are rophitine bees), but species of *Townsendiella* are parasites on bees of two separate families: *Hesperapis* (Melittidae) and *Conanthalictus* Cockerell, 1901 (Halictidae, Rophitinae). *Neolarra* in turn is very different because they seem to only attack *Perdita* (Andrenidae; Rozen 2000). This is interesting because *Perdita* is much younger than *Neolarra*, implying a rather recent host switch. *Perdita* diverged from *Macrotera* ~12 mya (stem age 24 mya; Cardinal et al. 2018), whereas we estimated a stem age of ~47 million years for *Neolarra*. This means that the MRCA of *Neolarra* must have used a different host lineage before *Perdita* originated. However, since we included a single representative of *Neolarra* for our molecular study, we cannot estimate a crown age for the group and can therefore not establish if the stem lineage of *Neolarra* diversified after the MRCA of present-day *Perdita* became a suitable host.

Other host–parasite relationships follow the general pattern of an earlier origin of the host lineage, followed by the origin of their respective parasites. A special case is the young age of *Protodufourea* (~10 mya, Cardinal et al. 2018), which is host to the likely older *Rhopalolemma* (stem age of ~40 mya). However, even though the divergence of *Protodufourea* and its species-poor sister group *Xeralictus* Cockerell, 1927 was rather recent, its stem age is very old (~58 mya, Cardinal et al. 2018). Further, we have no crown age estimates for *Rhopalolemma*, and differences in the crown ages of the host and parasite lineage may not be as great as indicated by the stem age of ~40 mya. Lastly, it is plausible that a host–parasite relationship was already established before the divergence event between *Protodufourea* and *Xeralictus*.

To date, the host(s) of *Schwarzia* remain unknown. Eardley (2009) speculated that *Systropha* is likely host to the genus, as it is the only representative of Rophitinae in Eastern Africa. Bossert (2019) pursued this suggestion but was not able to recover any *Systropha* specimens in Malaise trap samples in which *Schwarzia* was found. This would have shown that they at least co-occur in the same habitats, making a host–parasite relationship more likely. This changed with the present study: during two separate collecting events with Malaise traps, we were able to recover both *Schwarzia* and *Systropha* in the same habitats. At Ukasi Hill, *Schwarzia gretae* and *S. icipensis* were collected concurrently with a female of a presumably undescribed species of *Systropha* (Supp Fig. 2 [online only]), and a female of *Systropha* (*Austrosystropha*) *aethiopica* Friese 1911 was collected together with *S. elizabethae* in the Kasaala area (Supp Fig. 3 [online only]). Interestingly, if *Systropha* is indeed the host of *Schwarzia*, then both *Biastes* and *Schwarzia* must have independently converged on this host lineage. The age of *Systropha* is younger (stem age of ~24 mya, Cardinal et al. 2018) than the divergence between *Schwarzia* and *Biastes* (~39 mya, Fig. 1), making it impossible that host usage of *Systropha* is an ancestral, phylogenetically conserved trait. This again underlines the strong affinity of Neolarrini to parasitize rophitine hosts.

Overlooked Diversity in Eastern Africa

Until the discovery of *Schwarzia* in 2009, Neolarrini as defined here (including all former Biastini, Fig. 2) was thought to be exclusively Holarctic (Eardley 2009). The molecular data presented herein not only confirms the presence of a much wider biogeographical distribution of this lineage, but further highlights an unexpected species diversity of this group in the Afrotropical realm. Based on just 19 collecting events during which *Schwarzia* has ever been collected, all

but one using traps, a total of five species has been found. Despite these rather limited efforts, the resulting species richness already equals the sum of all known *Biastes* species of the remaining Old World. This makes it plausible that the highest species richness of this group could actually be in Eastern Africa. Furthermore, the COI sequence divergence between the species of *Schwarzia* are substantial (Table 2), clearly supporting the species status of the newly described bees.

Of particular importance for studying the largely unknown biology of the genus is the area on and around Ukasi Hill (Figs. 3 and 4A and B), which is home to three out of the five known species. This rather small area clearly represents a key locality to study *Schwarzia* and its yet to be discovered host(s). Situated in the former Eastern Province of Kenya near Ukasi town, Ukasi Hill is characterized by very dry and hot, xeric climatic conditions, with seasonal rainfalls (described in detail by Copeland et al. 2011). The area has been the collecting site of a number of extraordinarily rarely collected insects (e.g., Londt and Copeland 2017, Delvare and Copeland 2018, Pauly and Copeland 2019) and the rediscovery of the sole species of the fly family Mormotomyiidae (*Mormotomyia hirsuta* Austen; the 'terrible hairy fly') over 60 yr after the most recent sightings led to undertakings promoting the importance of this site for biological conservation (Copeland et al. 2011). The co-occurrence of these exceptionally rare insects highlights the need for continued efforts to study and improve our understanding of the Kenyan entomofauna and its significance for global insect biogeography.

Our newly presented records of *Schwarzia* increase the total number of collected specimens from 6 specimens and 3 collecting sites in 2009 (Eardley 2009) to 39 specimens and 16 sites in 2020. The distributional records of the genus indicate a preference for dry and hot climatic conditions, which is interestingly similar to those of other lineages of Neolarrini. While climatic preferences of these bees have not been comparatively studied, it seems obvious that they are predominantly present in xeric climates with short, seasonal rainfall. This is most clear for the North American lineages, which all occur in the arid and/or semi-arid regions of the continent, and *Townsendiella* and *Rhopalolemma* are only known from the deserts of the Southwestern United States and Northern and Central Mexico. Climatic preferences are less obvious for species of *Biastes* from the Old World, which have a wide distribution in Northern Eurasia and also occur in regions with year-round rainfall, such as Scandinavia or Middle Europe. In these regions however, finer-scaled distributional data shows *Biastes* and their hosts to occur primarily in locally drier and warmer localities (e.g., Amiet et al. 2007, Tischendorf et al. 2009, Westrich 2018). Understanding the climatic affinities of Neolarrini in a global context, including *Schwarzia* and its yet to be discovered host(s) represents an exciting avenue for future research.

In closing, we want to highlight the discovery of *Schwarzia* as a showcase for the undiscovered biodiversity of the rich and diverse habitats of Eastern Africa. Numerous ecosystems in Kenya and Tanzania exhibit a remarkable biodiversity of vertebrates, invertebrates and plants, as well as exceptional degrees of endemism (e.g., Myers et al. 2000, Burgess et al. 2007, Metcalfe et al. 2010, and literature cited therein). At the same time, many areas are severely impacted by anthropogenic habitat loss (e.g., Brooks et al. 2002, Metcalfe et al. 2010). In our case, very little effort revealed an unexpectedly diverse and ancient lineage of bees, with a still largely unknown biology. More undescribed species and likely even higher-level taxa can be expected to occur in the study areas but may also be threatened without being known to science.

Supplementary Data

Supplementary data are available at *Insect Systematics and Diversity* online.

The Supplemental Material contains a detailed version of the materials and methods, including the exact program versions and specific commands. Assembled DNA contig sequences, finalized alignments, phylogenetic trees, and the BEAST XML file are available from the figshare repository of this article (10.6084/m9.figshare.12890984). Unprocessed sequence data have been deposited in the NCBI Sequence Read Archive under BioProject PRJNA623013. Barcode sequences of *Schwarzia* can be accessed on the BOLD database using the specifiers listed under the species descriptions.

Acknowledgments

We thank Elizabeth Murray (Washington State University) for advice and her help with phylogenetic and biogeographical analyses. We further thank Erin Krichilsky and Kerrigan Tobin (USDA–ARS) for help with sample preparation, Matthew Buffington (USDA–ARS) for granting us access to the imaging system, and Peter Steward for collecting the single specimen of *Schwarzia lualenyiensis*. Robert L. Minckley (University of Rochester) kindly provided specimens used in this study. Parts of the laboratory work for this study was conducted in the L.A.B. facilities of the National Museum of Natural History, Smithsonian Institution. This work was supported by a U.S. National Science Foundation grant (DEB-1555905) to B.N.D., S.G.B., James P. Pitts, and Robert Ross, and Czech Science Foundation grant (20-14872S) to J.S., S.B. was supported by a Peter Buck fellowship at the Smithsonian Institution. Parts of the conducted phylogenetic analyses were carried out using the CIPRES Science Gateway (Miller et al. 2010). R.S.C. thanks the director of ICIPE for her continuing support of our project on the biodiversity of Kenyan insects, and he gratefully acknowledges the ICIPE core funding provided by UK Aid from the Government of the United Kingdom; Swedish International Development Cooperation Agency (SIDA); the Swiss Agency for Development and Cooperation (SDC); Federal Ministry for Economic Cooperation and Development (BMZ), Germany, and the Kenyan Government. USDA is an equal opportunity provider and employer.

Author Contributions

S.B., R.S.C., and J.S. conceptualized the project; S.B., T.J.L.S., J.P.G., M.G.B., S.G.B., B.N.D., J.P., and J.S. generated molecular data; S.B., R.S.C., J.P., J.S. conducted morphological analyses; S.B., T.J.L.S., J.P.G., M.G.B. processed sequence data; S.B. carried out phylogenetic analyses; S.B., R.S.C., T.J.L.S, M.G.B., S.G.B., B.N.D., J.S. interpreted the data; R.S.C., M.G.B., S.G.B., B.N.D. provided resources; S.B. generated illustrations; S.B. and J.S. led writing of the manuscript; all authors critically edited drafts and approved the final manuscript.

References Cited

Alexander, B. 1990. A cladistic analysis of the nomadine bees (Hymenoptera: Apoidea). Syst. Entomol. 15: 121–152.

Amiet, F., M. Herrmann, A. Müller, and R. Neumeyer. 2007. Fauna Helvetica, Apidae 5: *Ammobates, Ammobatoides, Anthophora, Biastes, Ceratina, Dasypoda, Epeoloides, Epeolus, Eucera, Macropis, Melecta, Melitta, Nomada, Pasites, Tetralonia, Thyreus, Xylocopa*, vol. 20. Schweizerische Entomologische Gesellschaft, Neuchâtel, Switzerland.

Andrews, S. 2019. FastQC: A quality control tool for high throughput sequence data. Accessed September 2019 on http://www.bioinformatics.babraham.ac.uk/projects/fastqc.

Ascher, J. S., and J. Pickering. 2020. Discover life bee species guide and world checklist (Hymenoptera: Apoidea: Anthophila). Accessed January 2020 on http://www.discoverlife.org/mp/20q?guide=Apoidea_species.

Bankevich, A., S. Nurk, D. Antipov, A. A. Gurevich, M. Dvorkin, A. S. Kulikov, V. M. Lesin, S. I. Nikolenko, S. Pham, and A. D. Prjibelski. 2012. SPAdes: a new genome assembly algorithm and its applications to single-cell sequencing. J. Comput. Biol. 19: 455–477.

Blaimer, B. B., M. W. Lloyd, W. X. Guillory, and S. G. Brady. 2016a. Sequence capture and phylogenetic utility of genomic ultraconserved elements obtained from pinned insect specimens. PLoS One 11: e0161531.

Blaimer, B. B., J. S. LaPolla, M. G. Branstetter, M. W. Lloyd, and S. G. Brady. 2016b. Phylogenomics, biogeography and diversification of obligate mealybug-tending ants in the genus *Acropyga*. Mol. Phylogenet. Evol. 102: 20–29.

Bogusch, P. 2003. Hosts, foraging behaviour and distribution of six species of cleptoparasitic bees of the subfamily Anthophorinae (Hymenoptera: Apidae). Acta Soc. Zool. Bohem. 67: 65–70.

Borowiec, M. L. 2016. AMAS: a fast tool for alignment manipulation and computing of summary statistics. PeerJ. 4: e1660.

Borowiec, M. L. 2019. Spruceup: fast and flexible identification, visualization, and removal of outliers from large multiple sequence alignments. J. Open Source Softw. 4: 1635.

Borowiec, M. L., E. K. Lee, J. C. Chiu, and D. C. Plachetzki. 2015. Extracting phylogenetic signal and accounting for bias in whole-genome data sets supports the Ctenophora as sister to remaining Metazoa. BMC Genom. 16: 1–15.

Bossert, S. 2019. Monotypic no more – a new species of the unusual genus *Schwarzia* (Hymenoptera, Apidae, Biastini). J. Hymenopt. Res. 69: 23–37.

Bossert, S. 2020. Data from: Phylogenomic and morphological reevaluation of the bee tribes Biastini, Neolarrini, and Townsendiellini (Hymenoptera: Apidae) with description of three new species of *Schwarzia*. Figshare. 10.6084/m9.figshare.12890984.

Bossert, S., E. A. Murray, E. A. B. Almeida, S. G. Brady, B. B. Blaimer, and B. N. Danforth. 2019. Combining transcriptomes and ultraconserved elements to illuminate the phylogeny of Apidae. Mol. Phylogenet. Evol. 130: 121–131.

Bouckaert, R., T. G. Vaughan, J. Barido-Sottani, S. Duchêne, M. Fourment, A. Gavryushkina, J. Heled, G. Jones, D. Kühnert, N. De Maio, et al. **2019**. BEAST 2.5: an advanced software platform for Bayesian evolutionary analysis. PLoS Comput. Biol. 15: e1006650.

Branstetter, M. G., J. T. Longino, P. S. Ward, and B. C. Faircloth. 2017. Enriching the ant tree of life: enhanced UCE bait set for genome-scale phylogenetics of ants and other Hymenoptera. Methods Ecol. Evol. 8: 768–776.

Brooks, T. M., R. A. Mittermeier, C. G. Mittermeier, G. A. B. Da Fonseca, A. B. Rylands, W. R. Konstant, P. Flick, J. Pilgrim, S. Oldfield, G. Magin, et al. **2002**. Habitat loss and extinction in the hotspots of biodiversity. Conserv. Biol. 16: 909–923.

Burgess, N. D., T. M. Butynski, N. J. Cordeiro, N. H. Doggart, J. Fjeldså, K. M. Howell, F. B. Kilahama, S. P. Loader, J. C. Lovett, B. Mbilinyi, et al. **2007**. The biological importance of the Eastern Arc Mountains of Tanzania and Kenya. Biol. Conserv. 134: 209–231.

Cane, J. H. 1983. Preliminary chemosystematics of the Andrenidae and exocrine lipid evolution of the short-tongued bees (Hymenoptera: Apoidea). Syst. Zool. 32: 417–430.

Capella-Gutiérrez, S., J. M. Silla-Martínez, and T. Gabaldón. 2009. trimAl: a tool for automated alignment trimming in large-scale phylogenetic analyses. Bioinformatics. 25: 1972–1973.

Cardinal, S., and B. N. Danforth. 2013. Bees diversified in the age of eudicots. Proc. R. Soc. B. 280: 1–9.

Cardinal, S., J. Straka, and B. N. Danforth. 2010. Comprehensive phylogeny of apid bees reveals the evolutionary origins and antiquity of cleptoparasitism. Proc. Natl. Acad. Sci. U.S.A. 107: 16207–16211.

Cardinal, S., S. L. Buchmann, and A. L. Russell. 2018. The evolution of floral sonication, a pollen foraging behavior used by bees (Anthophila). Evolution. 72: 590–600.

Castresana, J. 2000. Selection of conserved blocks from multiple alignments for their use in phylogenetic analysis. Mol. Biol. Evol. 17: 540–552.

Copeland, R. S., A. H. Kirk-Spriggs, S. Muteti, W. Booth, and B. M. Wiegmann. 2011. Rediscovery of the 'terrible hairy fly', *Mormotomyia hirsuta* Austen (Diptera: Mormotomyiidae), in eastern Kenya, with notes on biology, natural history, and genetic variation of the Ukasi Hill population. Afr. Invertebr. 52: 363–390.

Davis, C. C., C. D. Bell, S. Mathews, and M. J. Donoghue. 2002. Laurasian migration explains Gondwanan disjunctions: evidence from Malpighiaceae. Proc. Natl. Acad. Sci. U.S.A. 99: 6833–6837.

Dehon, M., A. Perrard, M. S. Engel, A. Nel, and D. Michez. 2017. Antiquity of cleptoparasitism among bees revealed by morphometric and phylogenetic analysis of a Paleocene fossil nomadine (Hymenoptera: Apidae). Syst. Entomol. 42: 543–554.

Delvare, G., and R. S. Copeland. 2018. Four-horned wasps, description of some remarkable *Dirhinus* (Hymenoptera, Chalcididae) from Kenya, with a discussion of their taxonomic placement. Zootaxa. 4374: 301–349.

Eardley, C. 2009. First record of the tribe Biastini from the Afrotropical Region (Hymenoptera: Apidae). Zootaxa 2264: 65–68.

Faircloth, B. C. 2013. Illumiprocessor: a trimmomatic wrapper for parallel adapter and quality trimming Version 2.0.9. GitHub, May 26, 2018. dx.doi.org/10.6079/J9ILL.

Faircloth, B. C. 2016. PHYLUCE is a software package for the analysis of conserved genomic loci. Bioinformatics. 32: 786–788.

Faircloth, B. C., M. G. Branstetter, N. D. White, and S. G. Brady. 2015. Target enrichment of ultraconserved elements from arthropods provides a genomic perspective on relationships among Hymenoptera. Mol. Ecol. Resour. 15: 489–501.

Fox, W. J. 1894. A proposed classification of the fossorial Hymenoptera of North America. Proc. Acad. Nat. Sci. Philadelphia. 46: 292–307.

Friese, H. 1895. Die Bienen Europa's (Apidae europaeae) nach ihren Gattungen, Arten und Varietäten auf vergleichend morphologisch-biologischer Grundlage, Theil I: Schmarotzerbienen. R. Friedländer & Sohn, Berlin, Germany.

GBIF. 2019. Custom data export (6th November 2019). Occurences of *Neopasites* spp. Accessed November 2019 under https://doi.org/10.15468/dl.lplh99 and https://doi.org/10.15468/dl.kv9knn.

Glenn, T. C., R. A. Nilsen, T. J. Kieran, J. G. Sanders, N. J. Bayona-Vásquez, J. W. Finger, T. W. Pierson, K. E. Bentley, S. L. Hoffberg, S. Louha, et al. **2019**. Adapterama I: universal stubs and primers for 384 unique dual-indexed or 147,456 combinatorially-indexed Illumina libraries (iTru & iNext). PeerJ. 7: e7755.

Grab, H., M. G. Branstetter, N. Amon, K. R. Urban-Mead, M. G. Park, J. Gibbs, E. J. Blitzer, K. Poveda, G. Loeb, B. N. Danforth. 2019. Agriculturally dominated landscapes reduce bee phylogenetic diversity and pollination services. Science. 363:282–284.

Heinrich, J. 1977. 1. Beitrag zur Kenntnis der türkischen Schmarotzerbienen. Nachr. Naturwiss. Mus. Aschaffenb. 85: 7–41.

Hoang, D. T., O. Chernomor, A. von Haeseler, B. Q. Minh, and L. S. Vinh. 2018. UFBoot2: improving the ultrafast bootstrap approximation. Mol. Biol. Evol. 35: 518–522.

Janzon, L.-Å., and B. G. Svensson. 1984. Aculeate Hymenoptera from a sandy area on the island of Oeland, Sweden. Nova Acta R. Soc. Scient. upsal. Ser.V: C, 3: 181–188.

Kalyaanamoorthy, S., B. Q. Minh, T. K. F. Wong, A. von Haeseler, and L. S. Jermiin. 2017. ModelFinder: fast model selection for accurate phylogenetic estimates. Nat. Methods. 14: 587.

Katoh, K., and D. M. Standley. 2013. MAFFT multiple sequence alignment software version 7: improvements in performance and usability. Mol. Biol. Evol. 30: 772–780.

Krombein, K. V., P. D. Hurd, D. R. Smith, and B. D. Burks. 1979. Catalog of Hymenoptera in America North of Mexico, vol. 2, Smithsonian Institution Press, Washington, DC.

Landis, M. J., N. J. Matzke, B. R. Moore, and J. P. Huelsenbeck. 2013. Bayesian analysis of biogeography when the number of areas is large. Syst. Biol. 62: 789–804.

Lanfear, R., P. B. Frandsen, A. M. Wright, T. Senfeld, and B. Calcott. 2016. PartitionFinder 2: new methods for selecting partitioned models of evolution for molecular and morphological phylogenetic analyses. Mol. Biol. Evol. 34: 772–773.

Linsley, E. G., and C. D. Michener. 1939. A generic revision of the North American Nomadidae (Hymenoptera). T. Am. Entomol. Soc. 65: 265–305.

Litman, J. R., C. J. Praz, B. N. Danforth, T. L. Griswold, and S. Cardinal. 2013. Origins, evolution, and diversification of cleptoparasitic lineages in long-tongued bees. Evolution. 67: 2982–2998.

Londt, J. G. H., and R. S. Copeland. 2017. *Nanoculcita*, a new genus of Afrotropical robber fly from Kenya (Asilidae: Stichopogoninae). Afr. Entomol. 25: 292–301.

Martins, A. C., D. R. Luz, and G. A. R. Melo. 2018. Palaeocene origin of the neotropical lineage of cleptoparasitic bees Ericrocidini-Rhathymini (Hymenoptera, Apidae). Syst. Entomol. 43: 510–521.

Matzke, N. J. 2018. BioGeoBEARS: BioGeography with Bayesian (and likelihood) evolutionary analysis with R scripts. version 1.1.1 published on GitHub on November 6, 2018. doi:10.5281/zenodo.1478250.

Metcalfe, K., R. Ffrench-Constant, and I. Gordon. 2010. Sacred sites as hotspots for biodiversity: the Three Sisters Cave complex in coastal Kenya. Oryx. 44: 118–123.

Michener, C. D. 1936. Some California bees, *Townsendiella* and *Hesperapis* (Hymen.: Apoidea). Entomol. News. 47: 181–185.

Michener, C. D. 1939. A revision of the genus *Neolarra* (Hymenoptera: Nomadidae). T. Am. Entomol. Soc. 65: 347–362.

Michener, C. D. 1979. Biogeography of the bees. Ann. Mo. Bot. Gard. 66: 277–347.

Michener, C. D. 2007. The bees of the world. The Johns Hopkins University Press, Baltimore, MD.

Miller, M. A., W. Pfeiffer, and T. Schwartz. 2010. Creating the CIPRES Science Gateway for inference of large phylogenetic trees. *In* 2010 Gateway Computing Environments Workshop (GCE), New Orleans, LA, 2010. pp. 1–8. doi:10.1109/GCE.2010.5676129.

Milne, R. I. 2006. Northern hemisphere plant disjunctions: a window on Tertiary land bridges and climate change? Ann. Bot. 98: 465–472.

Mitra, A. 2013. Function of the Dufour's gland in solitary and social Hymenoptera. J. Hymenopt. Res. 35: 33–58.

Morawitz, F. 1873. Nachtrag zur Bienenfauna des Gouvernements von St. Petersburg. Horae Societatis Entomologicae Rossicae. 9: 151–159.

Myers, N., R. A. Mittermeier, C. G. Mittermeier, G. A. Da Fonseca, and J. Kent. 2000. Biodiversity hotspots for conservation priorities. Nature. 403: 853–858.

Nguyen, L.-T., H. A. Schmidt, A. von Haeseler, and B. Q. Minh. 2015. IQ-TREE: a fast and effective stochastic algorithm for estimating maximum-likelihood phylogenies. Mol. Biol. Evol. 32: 268–274.

Orr, M., and T. Griswold. 2015. A review of the cleptoparasitic bee genus *Townsendiella* (Apidae, Nomadinae, Townsendiellini), with the description of a new species from Pinnacles National Park. ZooKeys 546: 87–104.

Pauly, A., and R. S. Copeland. 2019. *Meganomia somalica* (Friese, 1915) comb. nov. and new records of Meganomiinae for East Africa (Hymenoptera: Apoidea: Melittidae). Belg. J. Entomol. 89: 1–22.

Payne, A. 2014. Resolving the relationships of apid bees (Hymenoptera: Apidae) through a direct optimization sensitivity analysis of molecular, morphological, and behavioural characters. Cladistics. 30: 11–25.

Policarová, J., S. Cardinal, A. C. Martins, and J. Straka. 2019. The role of floral oils in the evolution of apid bees (Hymenoptera: Apidae). Biol. J. Linn. Soc. 128: 486–497.

Popov, V. V. 1933. Zametka o paraziticheskih pchelah roda *Biastes* Panz. (Hymenoptera, Nomadidae) [Notes on the parasititic bees allied to the genus *Biastes* Panz. (Hymenoptera, Nomadidae)]. Trudy Zoologicheskogo Instituta AN SSSR. 2: 51–75. [in Russian]

Proshchalykin, M. Y., and A. S. Lelej. 2004. New and little known Bees (Hymenoptera: Colletidae, Apidae) from the Russian Far East. Far East. Entomol. 136: 1–10.

Radoszkowski, O. 1874. Supplément indispensable à l'article publié par M. Gerstaecker, en 1869, sur quelques genres d'Hyménoptères. Bull. Soc. Nat. Moscou. 48: 132–164.

Rambaut, A., A. J. Drummond, D. Xie, G. Baele, and M. A. Suchard. 2018. Posterior summarization in Bayesian phylogenetics using Tracer 1.7. Syst. Biol. 67: 901–904.

Ratnasingham, S., and P. D. N. Hebert. 2007. BOLD: the barcode of life data system (http://www.barcodinglife.org). Mol. Ecol. Notes. 7: 355–364.

Ree, R. H., and I. Sanmartín. 2018. Conceptual and statistical problems with the DEC+J model of founder-event speciation and its comparison with DEC via model selection. J. Biogeogr. 45: 741–749.

Ree, R. H., and S. A. Smith. 2008. Maximum likelihood inference of geographic range evolution by dispersal, local extinction, and cladogenesis. Syst. Biol. 57: 4–14.

Roig-Alsina, A. 1991. Cladistic analysis of the Nomadinae s. str. with description of a new genus (Hymenoptera: Anthophoridae). J. Kans. Entomol. Soc. 64: 23–37.

Roig-Alsina, A., and C. D. Michener. 1993. Studies of the phylogeny and classification of long-tongued bees (Hymenoptera: Apoidea). Univ. Kans. Sci. Bull. 55: 123–162.

Ronquist, F. 1997. Dispersal-vicariance analysis: a new approach to the quantification of historical biogeography. Syst. Biol. 46: 195–203.

Rozen, J. G. 1966. The larvae of the Anthophoridae (Hymenoptera, Apoidea) part 2. The Nomadinae. Am. Mus. Novit. 2244: 1–38.

Rozen, J. G. 1996. Phylogenetic analysis of the cleptoparasitic bees belonging to the Nomadinae based on mature larvae (Apoidea, Apidae). Am. Mus. Novit. 3180: 1–39.

Rozen, J. G. 2000. Pupal descriptions of some cleptoparasitic bees (Apidae), with a preliminary generic key to pupae of cleptoparasitic bees (Apoidea). Am. Mus. Novit. 2000: 1–19.

Rozen, J. G. 2001. A taxonomic key to mature larvae of cleptoparasitic bees (Hymenoptera: Apoidea). Am. Mus. Novit. 2001: 1–28.

Rozen, J. G. J., and R. J. McGinley. 1991. Biology and larvae of the cleptoparasitic bee *Townsendiella* pulchra and nesting biology of its host *Hesperapis larreae* (Hymenoptera: Apoidea). Am. Mus. Novit. 3005: 1–11.

Rozen, J. G., and H. Özbek. 2003. Oocytes, eggs, and ovarioles of some long-tongued bees (Hymenoptera: Apoidea). Am. Mus. Novit. 2003: 1–35.

Rozen, J. G., K. R. Eickwort, and G. C. Eickwort. 1978. The bionomics and immature stages of the cleptoparasitic bee genus *Protepeolus* (Anthophoridae, Nomadinae). Am. Mus. Novit. 2640: 1–24.

Rozen, J. G., A. Roig-Alsina, and B. A. Alexander. 1997. The cleptoparasitic bee genus *Rhopalolemma*, with reference to other Nomadinae (Apidae), and biology of its host *Protodufourea* (Halictidae, Rophitinae). Am. Mus. Novit. 3194: 1–28.

Rozen, J. G., J. Straka, and K. Rezkova. 2009. Oocytes, larvae, and cleptoparasitic behavior of *Biastes emarginatus* (Hymenoptera: Apidae: Nomadinae: Biastini). Am. Mus. Novit. 2009: 1–15.

Scheuchl, E. 1995. Illustrierte Bestimmungstabellen der Wildbienen Deutschlands und Österreichs Band I: Schlüssel der Gattungen und der Arten der Familie Anthophoridae. Eigenverlag, Velden, Germany.

Scheuchl, E., and W. Willner. 2016. Taschenlexikon der Wildbienen Mitteleuropas. Quelle & Meyer Verlag, Wiebelsheim, Germany.

Shanks, S. S. 1978. A revision of the cleptoparasitic bee genus *Neolarra*. Wasmann J. Biol. 35: 212–246.

Shorthouse, D. P. 2010. SimpleMappr, an online tool to produce publication-quality point maps. Accessed April 2020 on http://www.simplemappr.net.

Straka, J., and P. Bogusch. 2007. Phylogeny of the bees of the family Apidae based on larval characters with focus on the origin of cleptoparasitism (Hymenoptera: Apiformes). Syst. Entomol. 32: 700–711.

Talavera, G., and J. Castresana. 2007. Improvement of phylogenies after removing divergent and ambiguously aligned blocks from protein sequence alignments. Syst. Biol. 56: 564–577.

The Angiosperm Phylogeny Group, Chase, M. W., M. J. M. Christenhusz, M. F. Fay, J. W. Byng, W. S. Judd, D. E. Soltis, D. J. Mabberley, A. N. Sennikov, P. S. Soltis, and P. F. Stevens. 2016. An update of the Angiosperm Phylogeny Group classification for the orders and families of flowering plants: APG IV. Bot. J. Linn. Soc. 181: 1–20.

Tiffney, B. H. 1985. The Eocene North Atlantic Land Bridge: its importance in Tertiary and modern phytogeography of the northern hemisphere. J. Arnold Arboretum. 66: 243–273.

Tischendorf, S., U. Frommer, H.-J. Flügel, K.-H. Schmalz, and W. Dorow. 2009. Kommentierte Rote Liste der Bienen Hessens: Artenliste, Verbreitung, Gefährdung, 1. Fassung. Hessisches Ministerium für Umwelt, Energie, Landwirtschaft und Verbraucherschutz, Wiesbaden, Germany.

Torchio, P. F., J. G. Rozen Jr, G. E. Bohart, and M. S. Favreau. 1967. Biology of *Dufourea* and of its cleptoparasite, *Neopasites* (Hymenoptera: Apoidea). J. N. Y. Entomol. Soc. 75: 142.

Warncke, K. 1981. Die Bienen des Klagenfurter Beckens (Hymenoptera, Apidae). Carinthia II. 171: 275–348.

Warncke, K. 1982. Zur Systematik der Bienen – Die Unterfamilie Nomadinae (Hymenoptera, Apidae). Entomofauna 3: 97–126.

Westrich, P. 1990. Die Wildbienen Baden-Württembergs, Spezieller Teil: Die Gattungen und Arten, 2nd ed. Ulmer, Stuttgart, Germany.

Westrich, P. 2018. Die Wildbienen Deutschlands. Eugen Ulmer KG, Stuttgart, Germany.